

1 EcoTWIN 1.0: A Fully Distributed Tracer-Aided Ecohydrological Model Tracking Water, 2 Isotopes, and Nutrients

3 Songjun Wu¹, Doerthe Tetzlaff^{1,2}, Yi Zheng³, Chris Soulsby⁴

4 1 Department of Ecohydrology and Biogeochemistry, Leibniz Institute of Freshwater Ecology and
5 Inland Fisheries, Berlin, Germany

6 2 Geography Institute and IRI THESys, Humboldt University of Berlin, Berlin, Germany

7 3 School of Environmental Science and Engineering, Southern University of Science and Technology,
8 Shenzhen, China

9 4 Northern Rivers Institute, School of Geosciences, University of Aberdeen, UK

10 Corresponding author: Songjun Wu (songjun.wu@igb-berlin.de)

11

12 Abstract

13 The value of stable water isotopes in constraining process representation in hydrological models is
14 well acknowledged with numerous tracer-aided hydrological models developed in recent years, yet
15 few have leveraged these benefits for more robust water quality modelling. Therefore, we introduce
16 EcoTWIN, a fully distributed tracer-aided ecohydrological model that simultaneously **tracks water,**
17 **isotopic isotope,** and **nutrient** fluxes ~~in an integrated C++ framework.~~ A thorough ~~validation model test~~
18 was conducted by calibrating EcoTWIN against discharge, in-stream isotopes, and NO₃-N
19 concentrations (1980-2024) in 17 large-scale (10³ - 10⁵ km²) European catchments spanning a wide
20 range of geographic and climatic gradients. Furthermore, three reanalysis products (ERA5 snow depth,
21 MODIS evapotranspiration, and GRACE surface water anomaly) were employed to further validate the
22 capacity of EcoTWIN to reproduce associated ~~but uncalibrated~~ internal water fluxes ~~without~~
23 ~~calibration~~. Results showed good model performance of both calibrated in-stream targets and
24 uncalibrated internal fluxes in most catchments. Therefore, we conclude that EcoTWIN is a flexible,
25 transferable modelling tool for prediction and process inference in terrestrial ecosystems ranging from
26 boreal to subtropic climates. Constrained by tracer simulations, the model not only captures the
27 celerity, but also the velocity of hydrological fluxes, thus providing spatio-temporally-explicit
28 estimations of water ages and travel times. Such information provides opportunities to bridge
29 catchment hydrology and water quality by linking travel times with biogeochemical processing times.
30 We demonstrate this with a proof of concept using Damköhler Number in nitrogen modelling.

31

32 1 Introduction

33 The development of ecohydrological models has been accelerating in the recent decades towards
34 frameworks that are more **spatially** distributed (instead of lumped or semi-distributed) and complex
35 (integrating more ecohydrological processes) (Pechlivanidis et al., 2011; Wellen et al., 2015). A few
36 examples include SWAT (Arnold et al., 2012), HYPE (Lindström et al., 2010), and mHM-Nitrate (Yang
37 et al., 2018), which have been widely applied worldwide. As process-based models, they are used not

38 only as prediction tools for specific variables, but also as learning tools for model inference, i.e., to
39 track the internal states/fluxes from available observations (Wang et al., 2024). This, however, poses
40 challenges [due to the considerable uncertainties in model inference](#).

41 Inference of internal processes is naturally uncertain due to the lack of direct observations, though
42 such uncertainty can be ~~somehow~~ constrained [to some extent](#) by rigorous split-sample calibration and
43 validation. The reason we use “somehow” here is based on the fact that most models are calibrated
44 to a minimal number of variables, and 81% of calibrations used data from a single gauge (mostly at a
45 catchment outlet) as reviewed in Wellen et al., (2015). Additionally, from a technical perspective,
46 “equifinality” further adds to the inference uncertainty due to the potential misinformation in data
47 (uncertainty in model forcing and observations) and model structure (the use of simplified, abstract
48 mathematics to simulate real world processes) (Beven, 2006). This can result in inaccurate process
49 representations yielding deceptively good results through error compensation, thus leading to
50 overconfidence in a model's ability to reproduce within-basin dynamics (Wen et al., 2024; Wu et al.,
51 2025a). As acknowledged by the hydrological community, models calibrated solely against discharge
52 at the catchment outlet reflect only the celerity of hydrological systems (pressure wave propagation),
53 yet constituent transport in water quality modelling relies on the velocity (mass flux of the water)
54 (McDonnell & Beven, 2014). Failure to reconcile these differences can lead to questionable process
55 inferences from many ecohydrological and water quality models.

56 One way to strengthen model inference is to include auxiliary data for calibration (Efstratiadis &
57 Koutsoyiannis, 2010). However, there is a paradox in multi-criteria calibration, as on the one hand,
58 more auxiliary data will feed unique information to the calibration process, thus effectively
59 constraining the model behaviour from an ecohydrological perspective; yet on the other hand, it
60 increases the dimensionality of calibration thus resulting in degraded performance or failure of
61 calibration from a technical perspective. The “curse” of dimensionality in ecohydrological modelling is
62 universal for all the commonly used algorithms under both Bayesian and Pareto theories as
63 demonstrated in Wu et al., (2025c). Therefore, modellers should expect the selected auxiliary data to
64 contain as much information as possible (Nearing et al., 2020). For distributed modelling, the auxiliary
65 data should reflect the cumulative contribution of all upstream reaches/regions, rather than variables
66 that are highly dependent on local condition/processes (e.g. point-scale soil moisture and
67 evapotranspiration measurements etc.).

68 Stable water isotopes, in this context, have powerful potential in cumulative flux tracking. As
69 conservative tracers, ^2H and ^{18}O are independent of biogeochemical reactions and naturally integrate
70 landscape heterogeneity, thus providing effective constraints on spatially distributed (dis)connections
71 of hydrological flow paths as well as velocity of the hydrological systems which reflect flux-storage
72 interactions (Jung et al., 2025; Tetzlaff et al., 2015). The value of tracers has long been recognised by
73 hydrologists (Hooper et al., 1988), with many tracer-aided hydrological models developed and evolved
74 in recent years from lumped (Birkel et al., 2011; Godsey et al., 2010), to semi-distributed (van
75 Huijgevoort et al., 2016; Nan et al., 2021), and distributed structure (Kuppel et al., 2018; Remondi et
76 al., 2018). However, few attempts have been made to integrate a tracer-aided hydrological structure

77 into water quality modelling (Birkel & Soulsby, 2015; Jung et al., 2025), despite the need being evident
78 for nearly four decades (Neal et al., 1988). Moreover, existing pioneering models are mostly
79 conceptualised/lumped (Benettin et al., 2015; Dick et al., 2015) and/or loosely coupled via external
80 tracer/water quality modules (Pesántez et al., 2023; Yang et al., 2024; Zhang et al., 2020). The external
81 coupling of model chains transfer necessary internal states and fluxes between sub-models (e.g.
82 hydrological fluxes for constituent mixing in water quality or isotopic modules) ~~on-disk-via online in-~~
83 memory coupling (instead of ~~memoryoffline on-disk coupling~~), thus significantly increasing the
84 resources consumption in input/output operations. Such model chains, though ~~provide~~providing
85 useful scientific insights, can become problematic for large-scale applications owing to the exponential
86 growth in computational and storage requirements. Therefore, there remains a need to develop a
87 fully distributed, computationally efficient ecohydrological model that combines hydrological, isotopic,
88 and water quality simulations.

89 This research gap motivated the development of EcoTWIN, the model that we present in this paper.
90 To our knowledge, the model is one of the first distributed tracer-aided **ecohydrological** models that
91 **tracks water, isotopic, and nutrient** fluxes simultaneously in ~~an-integrated a~~ C++-based framework.
92 For a thorough testing of EcoTWIN, 17 large European catchments were selected for calibration
93 against discharge, in-stream isotopes, and NO₃-N concentrations. These catchments span over a wide
94 range of geographic (Alpine to lowland plain) and climatic (from snow-dominated to Mediterranean)
95 gradients. In addition, the robustness of modelled inference on uncalibrated internal fluxes were also
96 compared with three remote sensing products (snow depth, evapotranspiration, and water storage).
97 Given the overall good integrated performance in most catchments, EcoTWIN is presented as an
98 ecohydrological modelling framework applicable for terrestrial ecosystems ranging from boreal to
99 temperate and subtropical climates across a wide range of geographical environments. The
100 subsequent sections are organised as follows: Section 2 and 3 introduce the model structure of
101 EcoTWIN and details in calibration and validation; the model performance is shown in Section 4; in
102 Section 5 we show the advantages of a tracer-aided ecohydrological framework with an example of
103 how water ages bridge catchment hydrology and water quality models; finally, the current limitations
104 and planned future development of EcoTWIN are also discussed.

105

106 **2 Model description**

107 EcoTWIN is fully distributed ecohydrological model implemented in C++. The model consists of
108 hydrological, isotopic, and nitrogen modules, which simulate major ecohydrological states and fluxes
109 from canopy to groundwater (Figure 1). Aided ~~withby~~ tracer simulations, the model is
110 additionally able to track the water movement vertically and laterally via the calculation of water ages
111 and travel times. For detailed information of model parameters please refer to Table S1.

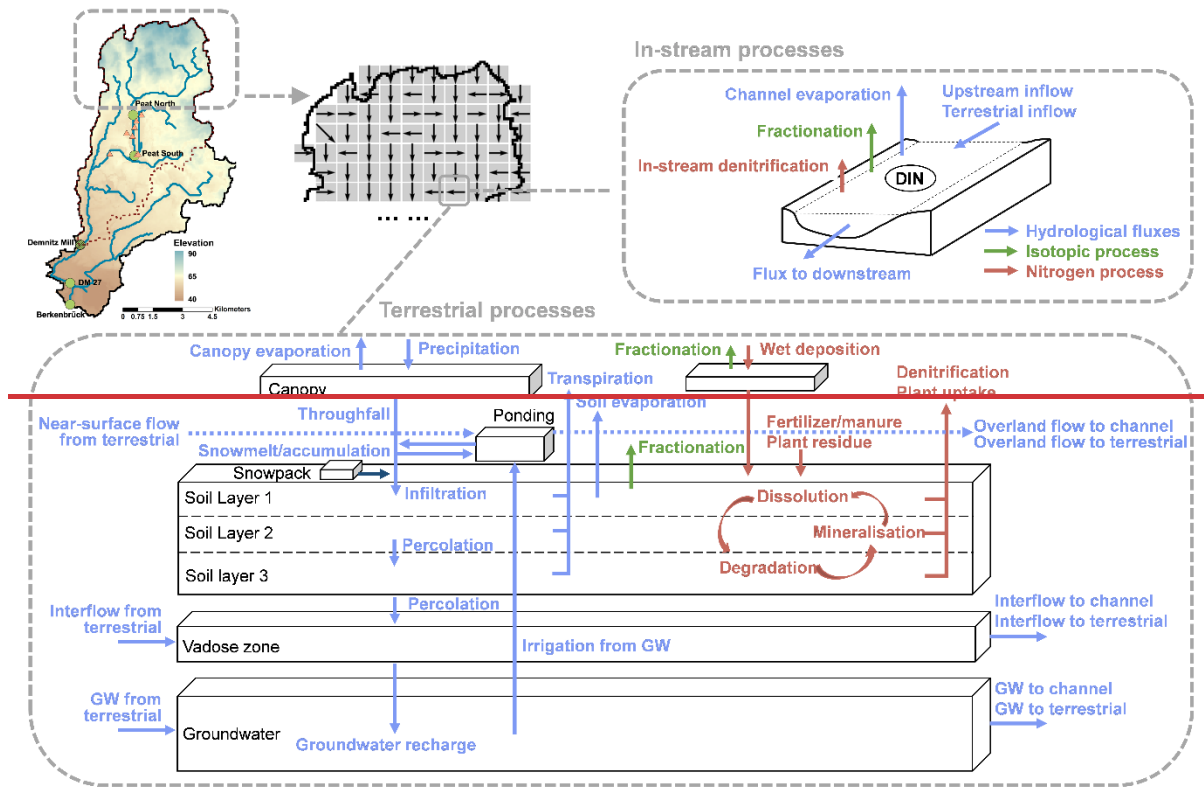


Figure 1. Model structure of EcoTWIN.

2.1 Hydrological module

EcoTWIN follows a typical multi-layer, top-down, bucket-type approach that resolves the water balance sequentially for the vegetation canopy, three soil layers, vadoseunsaturated zone, and groundwater. As the foundation of solute transport, the hydrological module employs a selective disassembly structure with multiple alternative conceptualisations possible for specific important hydrological processes. The configuration can be specified *a priori* based on the goal of modelling and prior knowledge of the studied catchment(s).

2.1.1 Soil properties

Before iterative simulations, soil characteristics are estimated using appropriate pedotransfer functions. Three different alternatives are provided, each of which requires different levels of inputs but all were found to provide robust estimation of soil porosity (θ_s), field capacity (θ_{fc}), wilting point (θ_{wp}), and hydraulic conductivity (K_s). All the soil properties are required for each soil layer/depth. This can be achieved via three alternative options: (i) assigning identical properties across the whole soil column, (ii) calculating separately for each depth based on depth-dependent inputs, or (iii) extrapolating deeper profile characteristics from the top soil properties based on a depth-dependent equation in Maneta & Silverman, (2013).

131 The distribution of soil types and land use ~~are~~ assigned from raster file in EcoTWIN. This can be
 132 specified as a static boundary condition; alternatively, the distributions can also be updated
 133 dynamically via a user-specified interval to reflect any temporal changes due to land management.

134

135 **2.1.2 Vertical fluxes**

136 The vertical fluxes are resolved for storages in the canopy, soil layers, ~~vadose~~unsaturated zone, and
 137 groundwater. The mass balance of canopy storage (ΔC) follows:

$$\Delta C = P - I - Th \quad (1)$$

138 where P , I , Th are precipitation, interception, and throughfall, respectively. The throughfall is
 139 calculated as the exceedance of current canopy storage from the maximum storage calculated by Leaf
 140 Area index LAI and a correlation parameter α .

$$C_{max} = \alpha * LAI \quad (2-1)$$

141 Alternatively, the maximum canopy storage can be estimated with explicit consideration of
 142 precipitation intensity (Landgraf et al., 2023):

$$C_{max} = \alpha * LAI * \left(1 - \frac{1}{1 + SCF * P / (\alpha * LAI)}\right) \quad (2-2)$$

143 where SCF is the vegetation cover fraction calculated by LAI and an extinction coefficient (rE)
 144 adopted from HYDRUS-1D (Šimůnek et al., 2013):

$$SFC = 1 - \exp(-rE * LAI) \quad (3)$$

145 Then throughfall is calculated as the exceedance of canopy storage from the maximum:

$$Th = (P + C) - C_{max} \text{ if } (P + C) > C_{max} \text{ else } 0 \quad (4)$$

146 After reaching land surface, throughfall becomes ponding water (S_{Pond}) or snow (S_{Snow}) depending
 147 on a temperature threshold for separation ($Thre_{SN}$). Snow will melt and recharge the ponding water
 148 in warm conditions (air temperature Ta exceed $Thre_{sn}$) following a degree-day model.

$$melt = S_{snow} * \min(dd_{min} + dd_{inc} * Th * (Ta - Thre_{SN}), dd_{max}) \quad (5)$$

149 Where dd_{min} and dd_{max} are the minimum and maximum of degree day factor, while dd_{inc} denotes
 150 the rate of increase in the degree-day factor per degree Celsius rise in temperature.

151 The available ponding water infiltrates into the top soil layer using Green-Ampt model (Kale & Sahoo,
 152 2011; Maneta & Silverman, 2013), with infiltration capacity first calculated as a function of average
 153 soil moisture over the hydrologically active depth:

$$I_f = K_s * \left(1 + \frac{\psi * \theta_s * (1 - (\theta_1 - \theta_{wt}) / (\theta_s - \theta_{wt}))}{\theta_1 * d_1}\right) \quad (6)$$

154 Where θ_1 , θ_s , θ_{wt} , and d_1 are the moisture content, porosity, wilting point, and depth in top soil layer;
 155 ψ is a parameter representing soil air entry pressure in m. Then potential infiltration (F_p) is determined

156 from the lesser between the available ponding water (S_{pd}) and potential infiltration rate integrated
 157 over time before ponding occurs ($I_f * t_p$).

158 The actual infiltration (F) is solved iteratively using the Newton–Raphson scheme:

$$F = \Delta\theta * d_1 = F_p + K_s * w_{Ks} * (\Delta t - t_p) - \psi\Delta\theta * \ln\left(\frac{\psi\Delta\theta + \Delta\theta d_1}{\psi\Delta\theta + F_p}\right) \quad (7)$$

159 where w_{Ks} is anisotropy ratio of vertical to horizontal K_s .

160 The soil storage in each layer is conceptualised as two water pools – a gravitational, free-flowing pool
 161 and a capillary, soil-bound pool. The two pools are separated based on field capacity (Maneta &
 162 Silverman, 2013), and percolation happens when soil storage exceeds the threshold. Three alternative
 163 schemes are included in EcoTWIN.

164 In the first scheme, all water in excess of field capacity percolates to deeper layer:

$$Pc_i = (\theta_i - \theta_{fc}) * d_i \quad (8-1)$$

165 where Pc_i , θ_i and d_i depict the percolation, moisture content and depth from/in i th soil layer in m.

166 The second scheme additionally considers the hydraulic conductivity (K_s) following the
 167 conceptualisation in SWAT (Arnold et al., 2012):

$$Pc_i = (\theta_i - \theta_{fc,i}) * d_i * (1 - \exp\left(\frac{-\Delta t * K_s}{\theta_{s,i} - \theta_{fc,i}}\right)) \quad (8-2)$$

168 The third scheme relates percolation to the extent of soil saturation with an exponential parameter β
 169 (Kumar et al., 2013; Samaniego et al., 2010):

$$Pc_i = (\theta_i - \theta_{fc,i}) * d_i * (1 - \exp(\beta * \log(\theta_i/\theta_{s,i}))) \quad (8-3)$$

170 For evapotranspiration, soil evaporation and transpiration are estimated separately. The separation
 171 of PET is realised by surface cover fraction introduced above:

$$PT = PET * SCF; \quad PE = PET - PT \quad (9)$$

172 Soil evaporation is simulated in the top soil layer based on the soil saturation:

$$Evap_s = PE * \min\left(\frac{\theta_1}{\theta_{fc,1}}, 1\right) \quad (10)$$

173 Transpiration is simulated in all soil layers based on the fractions ($f_{root,i}$) of root density ($D_{root,i}$) in
 174 each layer partitioned by soil depth and a parameter (γ_{root}):

$$Tr_i = PT * f_{root,i} * \frac{\theta_1 - \theta_{wp,1}}{\theta_{fc,1} - \theta_{wp,1}} \quad (11)$$

$$f_{root,i} = D_{root,i} / \sum_{j=1}^m D_{root,j} \quad (12)$$

$$D_{root,i} = \left(1 - \gamma_{root} \left(\sum_{j=1}^m d_j\right)\right) - \left(1 - \gamma_{root} \left(\sum_{j=1}^i d_j\right)\right) \quad (13)$$

175 Channel evaporation is also estimated using Penman equation, which relies on net radiation, wind
176 speed, air pressure, and air temperature as inputs.

177 The last soil layer percolates to an unsaturated storage in vadoseunsaturated zone ($S_{~~vadose~~unsat}$).
178 The compartment stores the excess water from soil and percolates either downward to groundwater
179 storage (S_{GW}) or laterally downstream. The percolation to groundwater $P_{c_{GW}}$ is determined by a
180 weighting parameter p_{GW} as a proportion of vadoseunsaturated storage:

$$P_{c_{GW}} = S_{~~vadose~~unsat} * p_{GW} \quad (14)$$

181 Additionally, irrigation is conceptualised in EcoTWIN, which is realised via the water extraction from
182 river or groundwater. The source is determined by the geographic location: for a grid cell with channel
183 network, water is extracted directly from river, and local groundwater is used as irrigation source for
184 non-channel grids. The amount of extraction is estimated from a predefine coefficient for crop water
185 demands (w_{irr}) from which the deficit is calculated for each of the m soil layers.

$$deficit = \sum_{i=1}^m (\theta_{fc,i} - \theta_{wp,i}) * w_{irr} * d_i \quad (15)$$

186 Note that the irrigation can switch to groundwater extraction if river storage cannot fill the deficit.

187

188 **2.1.3 Lateral fluxes**

189 In EcoTWIN, grid cells are connected laterally at three levels - surface, vadoseunsaturated zone, and
190 groundwater. Note that some models omit the vadose/unsaturated storage and directly calculate
191 excess water to drain based on the saturation extent of the bottom soil layer (e.g., Ech2O-iso, Kuppel
192 et al., 2018). EcoTWIN did not follow this conceptualisation because in reality, the lateral drainage is
193 focused in the saturated zone, and thus the bottom of the soil layer instead of the whole soil profile.
194 The drainage of an entire soil layer thus brings considerable uncertainty to the velocity of lateral
195 transport when the lower boundary of the soil is a parameter to tune in calibration. For instance, a
196 large soil depth will dramatically reduce the velocity of interflow drainage and slow down the mixing
197 of constituents, though this might still perfectly reproduce the celerity (hydrograph) for purely
198 hydrological modelling. Our conceptualisation (an independent unsaturated compartment) aligns
199 with most hydrological models (Arnold et al., 2012; Yang et al., 2018) and fits the recent analysis
200 supporting the dominant role of lateral drainage over vertical transports globally (Mcmillan et al.,
201 2025).

202 By the end of each timestep, ponding water receives upstream inputs and contributes to channel
203 storage if the grid is connected to the channel network, while non-channel grid has $Ovf_C = 0$:

$$Ovf_C = (Ovf_{T,in} + S_{pond}) * p_{ovf} * dx_C/dx_T \quad (16)$$

204 dx_C and dx_T are the channel length and size of terrestrial grid cell; p_{Ovf} is a weighting parameter for
 205 channel recharge. Then the remaining ponding water routes to downslope terrestrial grid following
 206 the topographic gradient. In none-channel grid cells, all available ponding storage routes lateral
 207 downstream ($Ovf_C = 0$):

$$Ovf_{T,out} = (Ovf_{T,in} + S_{pond}) - Ovf_C \quad (17)$$

208 Similarly, vadoseunsaturated storage contributes first to channel storage in grid cells within channel
 209 network, while non-channel grid cells have $Inf_C = 0$:

$$Inf_C = (Inf_{T,in} + S_{vadose}) * K_{vadose} * (1 - e^{-1 * exp_{Inf} * (Inf_{T,in} + S_{vadose})}) * p_{Inf} \quad (18)$$

210 where K_{vadose} is the effective conductivity of lateral transport in the vadoseunsaturated zone; while
 211 exp_{Inf} is an exponential parameter determining the strength of positive correlation between
 212 recharge and current vadoseunsaturated storage. Then the remaining vadoseunsaturated storage is
 213 partially routed to downslope grid cell following a linear approximation of Kinematic wave equation,
 214 which assumes gravitational flux per unit width $Inf_{T,out}$ is proportional to the subsurface hydraulic
 215 conductivity (K_{vadose}) and bedrock slope (*slope* approximated from the surface slope):

$$Inf_{T,out} = (\cancel{Inf_{T,in} + S_{vadose} - Inf_C})(Inf_{T,in} + S_{unsat} - Inf_C) * (1 + \alpha * \frac{dt}{dx}) * \alpha * \frac{dt}{dx} \quad (19)$$

$$\text{where } \alpha = \cancel{K_{vadose}} K_{unsat} * \sin(\text{slope})$$

216 Groundwater routing is similar to that of interflow, with channel recharge followed by terrestrial
 217 transport. Note that the terrestrial groundwater flow does not consider the bedrock slope as
 218 groundwater storage is generally much large than vadoseunsaturated storage, and thus independent
 219 from topographic gradients:

$$GWf_C = (GWf_{T,in} + S_{GW}) * K_{GW} * (1 - e^{-1 * exp_{GWf} * (GWf_{T,in} + S_{GW})}) * p_{GWf} \quad (20)$$

$$GWf_{T,out} = (GWf_{T,in} + S_{GW} - GWf_C) * (1 + \alpha * \frac{dt}{dx}) * \alpha * \frac{dt}{dx} \quad (21)$$

$$\text{where } \alpha = K_{vadose}$$

220 The channel routing is realised using Kinematic wave equation based on a scaled channel roughness
 221 parameter (Maneta & Silverman, 2013).

222

223 2.2 Isotopic module

224 The isotopic module in EcoTWIN tracks the composition of stable water isotopes in all water storage
 225 compartments following hydrological mixing and fractionation. The module also provides estimation
 226 of water age and travel time conceptualised as the time since water molecules enter the catchment
 227 as precipitation, and the time water molecules need to travel through the specific storage.

228 2.2.1 Mixing

229 The mixing and transport of isotopes (^2H and ^{18}O , both noted as C) are governed by the velocity of
230 hydrological fluxes with a complete mixing strategy for most water storages:

$$\frac{d(V * C)}{dt} = \sum_{k=1}^{N_{in}} q_{in,k} * C_{in,k} - \sum_{k=1}^{N_{out}} q_{out,k} * C \quad (22)$$

231 Where V and C are the volume and composition/concentration of the storage, while N_{in} and N_{out}
232 denote the number of influx and outflux. Such strategy is built on two assumptions: (i) constituents (i.e.,
233 isotopes) are fully mixing within each timestep; (ii) the composition/concentration in outflow equals
234 to that in storage. Additional mixing between ponding and upper soil water storage is allowed (with
235 proportion determined by a parameter *SrfMixing*), as nutrients in top soils can be flushed out in
236 large hydrological events (Seybold et al., 2022).

237 The full-mixing assumptions have been widely used and shown to be reasonable for storages with
238 relatively small volumes in many mixing/water quality models (Arnold et al., 2012; Yang et al., 2018).
239 However, some studies show that a complete mixing strategy can be problematic for large storages
240 such as groundwater (~~e.g. as they are generally poorly constrained (e.g.~~ Soulsby et al., 2015). Therefore,
241 the mass conservation equation used in the INCA-N model and mHM-Nitrate is employed to
242 ~~calculate~~ calculate the mixing of groundwater storages with influxes (i.e., percolation from
243 ~~vadose unsaturated~~ storage and lateral groundwater inflow).

$$\frac{dC}{dt} = \frac{1}{V + V_r} * \left(\sum_{k=1}^{N_{in}} q_{in,k} * C_{in,k} - \sum_{k=1}^{N_{out}} q_{out,k} * C \right) \quad (23)$$

244 where V_r is the retention storage. The equation is solved by the fourth order Runge-Kutta technique.

245

246 2.2.2 Fractionation

247 As conservative tracers, ~~the~~ composition of isotopes in water storages/fluxes is only ~~regulated~~ changed
248 by kinetic fractionation apart from hydrological mixing. The process is accompanied by evaporation,
249 resulting in the preferential loss of lighter isotopes (^1H and ^{16}O) to the vapor phase and a
250 corresponding enrichment of heavier isotopes (^{18}O and ^2H) in the residual water. In EcoTWIN, the
251 fractionation is simulated along with evaporation of top soil water and river storage based on the
252 Craig-Gordon model (Craig et al., 1964; Kuppel et al., 2018), while transpiration is assumed to be a
253 non-fractionating process (Dawson & Ehleringer, 1991; Kuppel et al., 2018).

$$C = C^* - (C^* - C) * \left(\frac{S - Evap}{S} \right)^m \quad (24)$$

254 where C^* and m are the limiting isotopic composition (in ‰) and the dimensionless enrichment slop
255 that are estimated via the following equations in (Good et al., 2014):

$$C^* = \frac{h_a C_a + h_s \varepsilon^+ + \varepsilon^k}{h_s - h_a + \varepsilon^k / 1000} \quad (25)$$

$$m = \frac{h_a - (h_s \varepsilon^+ + \varepsilon^k) / 1000}{h_s - h_a + \varepsilon^k / 1000} \quad (26)$$

256 where h_a is the relative humidity above the soil surface normalised from atmospheric relative
 257 humidity (h), air temperature (T_a), and soil temperature (T_s estimated from Amato & Giménez, 2024).
 258 C_a is the isotopic composition of ambient air moisture estimated from precipitation composition:

$$C_a = (C_{rain} - \varepsilon^+) / \alpha^+ \quad (27)$$

259 where ε^+ is the equilibrium fractionation factor (Skrzypek et al., 2015); α^+ is a temperature factor
 260 estimated from T_a .

$$\varepsilon^+ = (1 - 1/\alpha^+) * 1000 \quad (28)$$

261 The factor of diffusion-controlled kinetic isotopic separation ε^k is calculated based on the relative
 262 humidity of soil surface (h_a) and soil pore (h_s).

$$\varepsilon^k = (h_s - h_a) * \left(1 - \frac{D_i}{D}\right) * n \quad (29)$$

263 Where D_i and D denote the diffusivities of water vapor molecules containing heavier isotope and the
 264 lighter isotope, respectively. The ratio can be acquired in Horita et al., (2008) for ^2H (0.9877) and ^{18}O
 265 (0.9859). n is an advection term ranging between 0.5 (in saturated soils) and 1 (in dry soils). The factor
 266 is included in calibration for the fractionation of top soil evaporation yet fixed as 0.5 for that of channel
 267 evaporation.

268

269 **2.2.3 Water age and travel time**

270 EcoTWIN can track the age of water i.e., the time since water enters the catchment as precipitation,
 271 in each storage. In age tracking, precipitation is defined as new water with age of zero. At the end of
 272 each time step, water ages of all storages are advanced based on the temporal resolution (for instance
 273 one day if the model is set up for daily timesteps). Note that in some circumstances, the modellers
 274 might need to disable the age evolution of specific storage(s) (e.g., groundwater storage) as the
 275 storage can be too large to achieve steady states in model spin-up. Similar to isotopes, water ages are
 276 only controlled by hydrological transport with the same mixing strategy (i.e., complete mixing except
 277 for groundwater).

278 The water ages in EcoTWIN are the mean values averaged from all water molecules in the storage,
 279 which might be dominated by the inflow of very old water that obscure the age distribution of the
 280 young water (e.g., the groundwater input to top soils due to the groundwater extraction for irrigation).
 281 Therefore, EcoTWIN additionally provides the estimation of travel time - the time of water molecule
 282 travelling through each storage. The simulation is similar to that of water ages. The only difference is
 283 that the transition of water between storages (e.g., percolation into deeper soil layers) resets the travel

284 time to zero. Accordingly, all the water enters a new storage becomes new water instead of just
 285 precipitation in water age tracking.

286

287 **2.3 Nitrogen module**

288 The nitrogen module describes the mass balance of nitrogen, particularly nitrate as the main form of
 289 dissolved nitrogen, which is dominated by the interaction of hydrological transport and
 290 biogeochemical transformations.

291 For each timestep, the nitrate concentration is simulated in each storage following three processes –
 292 hydrological transport/mixing, nitrogen inputs, and biogeochemical transformations. Fully integrated
 293 with hydrological module, nitrate transport also aligns with hydrological fluxes following the same
 294 mixing strategy as in the isotopic simulation. For nitrogen sources, EcoTWIN considers the inputs from
 295 fertiliser, manure, and plant residues, whose annual inputs can be specified via configuration. Notably,
 296 fertilization can be parameterised via spatial raster inputs if corresponding dataset is available. The
 297 timing and extent of nitrogen addition of all sources are determined following the implementation in
 298 HYPE (Lindström et al., 2010), which distributes the annual sum across a specified period (e.g., the
 299 period between planting and harvest for crops). Additionally, wet deposition is conceptualised as the
 300 atmospheric nitrogen source, whose concentration can be specified via spatial raster and simply as a
 301 constant value.

302 The biogeochemical transformations are mainly modified from the mHM-Nitrate model (Yang et al.,
 303 2018), and the HYPE model (Lindström et al., 2010), which are conceptualised for [the](#) soil profile and
 304 channel network. In the soil profile, three nitrogen pools are conceptualised for each soil layer,
 305 including an inactive nitrogen pool (SN_i), an active nitrogen pool (SN_a), and a dissolved nitrate pool
 306 (DN). The soil transformations include degradation (Dgd_s , from SN_i to SN_a), mineralisation ($Minr_s$,
 307 from SN_a to DN), denitrification ($Deni_s$, from DN to gaseous N_2), and plant uptake ($Uptk_s$, DN
 308 removal).

$$Dgd_s = SN_i * ref_{Dgd,s} * f_{Ta} * f_{\theta} / dt \quad (30)$$

$$Minr_s = SN_a * ref_{Minr,s} * f_{Ta} * f_{\theta} / dt \quad (31)$$

$$Deni_s = DN * ref_{Deni,s} * f_{Ta} * f_{\theta,deni} * f_{conc,s} / dt \quad (32)$$

309 where $ref_{Dgd,s}$, $ref_{Minr,s}$, $ref_{Deni,s}$ are the parameters representing the reference rates of soil
 310 degradation, mineralisation, and denitrification. f_{Ta} and f_{θ} are the regulating factors of temperature
 311 and moisture.

$$f_{Ta} = 2^{(T_a - 20)/10} * \omega \quad \text{where } \omega = \begin{cases} 1 & T_a > 5 \\ T_a/5 & 0 \leq T_a \leq 5 \\ 0 & T_a < 0 \end{cases} \quad (33)$$

$$f_{\theta} = \min \left[\frac{(1 - p_{\theta,deni}) * (\theta_{fc,i} - \theta_i)}{p_{\theta,fc} * d_i}, \frac{(\theta_i - \theta_{wp,i})}{p_{\theta,wp} * d_i} \right] \quad (34)$$

312 where $p_{\theta,fc}$ and $p_{\theta,wp}$ are the empirical factors that are fixed as 1.2, 0.8 based on literature values
 313 (Lindström et al., 2010; Yang et al., 2018). $p_{\theta,deni}$ is the saturation threshold for soil denitrification
 314 ranging between 0.4 – 0.85 (Yang et al., 2018). A different moisture factor considering a saturation
 315 threshold (θ_{thres}) is employed for denitrification, as denitrification is more sensitive to the soil
 316 wetness condition:

$$f_{\theta,deni} = [(\theta_i/\theta_{fc,i} - \theta_{thres})/(1 - \theta_{thres})]^{2.5} \quad (35)$$

317 The process is additionally controlled by the concentration level in the storage $f_{conc,s} = C/(C + 10)$.
 318 Plant uptake is simulated using a three-parameter logistic growth equation in (Eckersten et al., 1994;
 319 Lindström et al., 2010).

320 Currently, in-stream denitrification is the only process considered in EcoTWIN.

$$Deni_w = ref_{Deni,w} * f_{T_w} * f_{conc,w} * A/dt \quad (36)$$

321 where $ref_{Deni,w}$ is the reference in-stream denitrification rates. The actual rates are regulated by a
 322 concentration factor $f_{conc,w} = C/(C + 1.5)$ and a temperature factor f_{T_w} (the same equation for f_{Ta}
 323 with inputs substituted by river temperature f_{T_w} , simplified as the rolling-average of 20-day air
 324 temperature).

325 It should be noted that the calibrated soil depth in this study is about 2.5 m, with intermittent
 326 saturation occurring in the deeper layer. This means that terrestrial denitrification is a combination of
 327 soil and groundwater processes in this study, though this might change in other applications if a
 328 shallow soil depth is assigned.

329

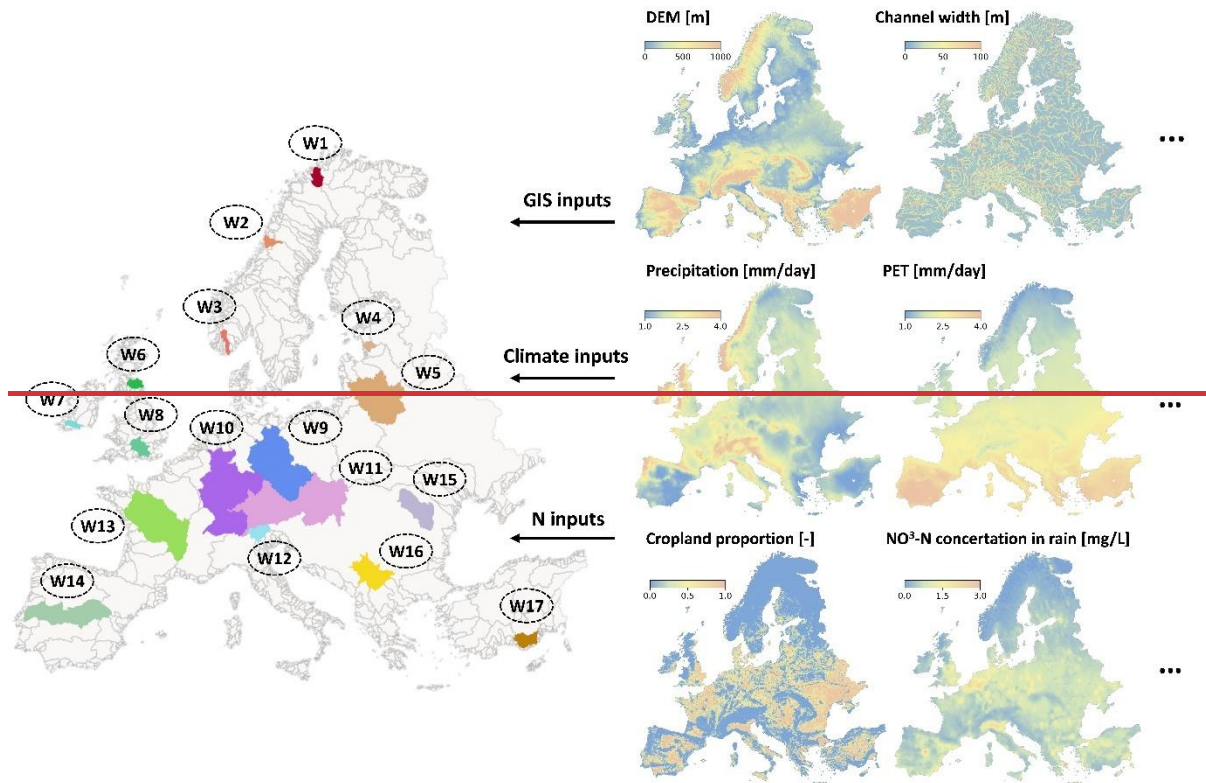
330 **3 Model calibration and validation**

331 To examine the capacity of EcoTWIN to ~~A robust model application should not only~~ reproduce
 332 ecosystem functioning, observed variables through calibration but also yield realistic estimates of
 333 internal states and fluxes that are not included in the calibration process. This is essential to avoid
 334 situations where inaccurate process representations produce deceptively good results through error
 335 compensation. Therefore, we evaluate EcoTWIN from both perspectives. First, we assess the model is
 336 tested and validated via two aspects – (i) the’s ability to reproduce observations via calibration
 337 (methods and results in Sections 3.2 and 3.4). Then, we examine the model’s capacity to simulate
 338 uncalibrated internal states and fluxes by comparing the calibrated observations and (ii) to capture
 339 the general spatio-temporal patterns of internal fluxes with important ecohydrological implications
 340 yet not included in calibration (e.g., simulated snow depth, evapotranspiration), and total water
 341 storage with corresponding remote-sensing products (methods and results in Sections 3.3 and 3.5).

342 To ensure model generality, 17 catchments ~~are~~were selected for calibration and validation, depending
 343 on the data availability (particularly stream stable water isotopes and nitrate), which span a wide
 344 range of characteristics in geography, climate, and anthropogenic managements (Figure 2 and Table
 345 1). Anthropogenic management practices have a less dramatic effect than climate and geography in

346 most catchments due to the relatively low proportion of urbanized areas. However, a few notable
 347 exceptions—such as the Rhine, Elbe, and Danube catchments—are included in the analysis, as these
 348 densely populated regions hold critical ecological, agricultural, and economic importance for Europe,
 349 and are subject to intensive human interventions in water management. This also provides a chance
 350 to examine the applicability of EcoTWIN in human-affected catchments.

351



352

353 **Figure 2. The selected catchments for model validation and an overview of inputs.**

354

355 **Table 1. Characteristics of the selected catchments. Lat depicts the latitude of upper left corner of the**
 356 **catchment. DEM and Area are the mean elevation in m.a.s.l. and catchment size in km². Precip, Temp,**
 357 **and PET are the annual averages of precipitation, air temperature, and potential evapotranspiration**
 358 **in mm/yr. f_{crop} , f_{forest} , and f_{urban} are the fractions of cropland, forest, and urbanized areas in 2019**
 359 **in %. Null means no name is assigned for the catchment in the Catchment Characterisation and**
 360 **Modelling (CCM) database.**

ID	Name	Lat	Area	DEM	Precip	Temp	PET	f_{crop}	f_{forest}	f_{urban}
1	Null	70.0	8725	468.5	448.5	-1.8	442.8	<1	1.9	<1
2	Vefsna	65.9	5475	636.5	1260.8	0.7	433.6	<1	24.6	<1
3	Null	59.8	5225	742.3	1400.9	3.0	545.7	<1	39.8	<1
4	Null	58.3	4350	67.4	654.5	6.4	667.9	17.4	60.5	1.4
5	Nemunas	56.6	97550	147.9	599.3	7.1	730.6	33.0	39.1	4.5
6	Tweed	55.9	6250	264.3	1023.4	7.9	600.9	21.8	18.9	1.4
7	Null	52.3	4300	175.4	1218.1	10.1	645.2	12.1	17.4	1.9

8	Thames	52.2	11900	112.0	700.7	10.4	782.9	44.9	14.1	22.0
9	Elbe	53.5	130225	318.3	626.9	8.8	836.3	41.2	34.6	10.8
10	Rhine	52.0	170175	508.3	943.3	8.9	821.0	21.5	41.2	17.1
11	Danube _(w)	50.5	197600	618.0	843.6	8.3	857.4	28.5	37.1	11.5
12	Adige	47.2	11600	1771.0	1002.3	4.5	809.7	4.1	48.8	3.2
13	Loire	48.7	122125	298.9	778.7	11.0	887.4	37.6	25.7	6.5
14	Taje	40.4	75575	686.2	549.5	14.3	1359.6	26.7	34.5	3.3
15	Danube _(w)	48.4	37975	533.3	534.7	8.1	869.5	32.0	41.3	6.4
16	Danube _(w)	44.8	37725	653.3	684.7	9.7	994.2	12.8	44.3	5.8
17	Null	37.6	12650	1384.5	454.1	12.2	1256.9	5.9	4.3	4.1

361

362 **3.1 Model setup and calibration**

363 EcoTWIN was setup for each of the 17 catchments for calibration with a spatial resolution of 5 km²
364 and a temporal resolution of daily timesteps from 1980 to 2024. (with first two years for spin-up). As
365 a fully distributed model, gridded GIS inputs are used in the model setup, including a digital elevation
366 model, flow direction, slope, channel width, channel length, proportion of each land use type (Winkler
367 et al., 2021), proportions of each soil type (world soil map, WRB2014), and soil properties (e.g., depth-
368 dependent proportions of clay, sand, silt, and organic matter from SOILGRIDS). All spatial inputs were
369 acquired with finer resolution (50 m or above) and resampled to the resolution of this application (5
370 km).

371 The climatic variables used to drive EcoTWIN include precipitation, air temperature, potential
372 evapotranspiration, relative humidity, and a few variables that are optional required for the
373 calculation of channel evaporation (air pressure, net radiation, and wind speed). These climatic
374 variables are available from the reanalysis products ERA5 and E-OBS, while PET is calculated using FAO
375 Penman-Monteith equation. For nitrogen simulations, additional inputs are needed including the
376 fertilization map (Grizzetti et al., 2021) and nitrate concentration of rainfall (Zhu et al., 2025) as the
377 boundary of nitrogen addition from agricultural activities and wet deposition.

378

379 **3.2 Model calibration**

380 The calibration was conducted separately for each catchment to test the applicability of EcoTWIN
381 under different geological and climatic contexts. Three commonly used variables for hydrological and
382 water quality modelling (discharge, stream water isotope composition, and in-stream NO₃-N
383 concentrations) are employed for calibration. Their long-term time series were acquired at daily steps
384 from different sources (discharge from GRDC, isotopes from Wateriso and GNIR, and NO₃-N
385 concentration from global water quality database, GEMStat), and then compared with simulation
386 results at multiple sites for each catchment. Here ¹⁸O was selected for isotopic validation due to its
387 higher precision and data abundance. Given the discrepancy in duration of observations (especially
388 for isotopes and NO₃-N), a separate calibration and validation based on a split-sample approach is
389 difficult. Therefore, the full timescale (1982 - 2024) was used for calibration (and the validation
390 introduced in Section 3.23).

391 The Differential Evolution Adaptive Metropolis algorithm (DREAM) was selected for parameter
 392 optimisation due to its relatively efficient and effective performance for high-dimensional problems
 393 (as benchmarked in Wu et al., 2025c). The algorithm was implemented separately for each catchment
 394 with the same prior distribution of parameters (Table S1). The maximum iteration was set as 100,000
 395 for each catchment (20 chains with maximum chain length of 5000), from which 40 best simulations
 396 were selected from the posterior distribution. The Kling-Gupta efficiency (KGE) statistic was used to
 397 construct an informal likelihood function for DREAM optimisation.

$$398 \quad l = \left[\sum_{i=1}^{N_{obs}} \sum_{j=1}^{N_{site}} (1 - KGE) * w_{i,j} \right]^{-m}$$

$$399 \quad l = \left[\sum_{i=1}^{N_{obs}} \sum_{j=1}^{N_{site}} (1 - KGE) * w_{i,j} \right]^{-m} \quad (37)$$

399 Where *l* is the likelihood; N_{obs} and N_{site} are the number of observation types (3 discharge, isotopes,
 400 and nitrate) and sites. The weight $w_{i,j}$, defined for observation type i at site j , is assigned equally
 401 across sites such that the total weight for each observation type sums to 1/3. m is an exponentially
 402 coefficient to stretch the likelihood surface that is often set based on the number of observation points.
 403 After prior test run, m was set as 500. Finally, the likelihood function is transformed to logarithmic
 404 form for numeric stability. The calibration was validated using Kling-Gupta efficiency (KGE), Root Mean
 405 Square Error (RMSE), Pearson Correlation Coefficient (Coefficient), and Percent bias (Pbias) (Table 2).

407 **3.23 Model validation**

408 Reanalysis products were further employed to validate uncalibrated internal model states or fluxes
 409 from three important perspectives in ecohydrological modelling – snow depth from ERA5,
 410 evapotranspiration from MODIS, and surface water mass anomaly from GRACE (as a storage proxy).
 411 The simulated variables corresponding to these products are, respectively, the depth of snow pack,
 412 the sum of soil evaporation, channel evaporation, and transpiration from all soil layers, and the
 413 anomaly of total water storage above groundwater (i.e., the sum of canopy storage, snow, soil water
 414 storages, and vadoseunsaturated storage). The validation was realised via resampling the remote
 415 sensing products to 5 km and comparing grid-to-grid with the modelled outputs. Note that r^2 was used
 416 as the performance metrics, as KGE is not applicable for time series with zero average, yet the average
 417 of surface mass anomaly is close to 0.

419 **3.4 Results**

420 **4.1 Simulation Calibration performance**

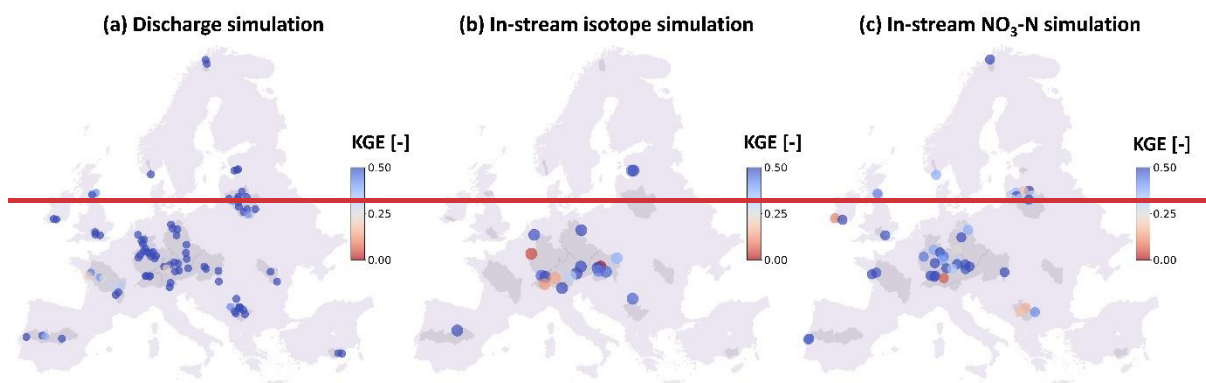
421 Generally, EcoTWIN successfully reproduced the observed discharge in all 17 catchments with KGE
 422 exceeding 0.5 at most site (Figure 3a). This is further demonstrated in Figure 4 where both seasonality

423 and peaks of discharge with different levels of magnitudes were captured. Such performance is at
424 least comparable to or better than previous continental calibration of hydrological models (e.g.,
425 ParFlow, Naz et al., 2023; E-HYPE, Donnelly et al., 2016).

426 Similarly, isotopic and nitrate simulations also produced good performances at most sites (Figure 3b).
427 However, there are a few exceptions. The failure of isotopic simulations was found at two sites within
428 the Alpine region (bottom left corner of figure 3b). This can be attributed to the uncertainty in
429 precipitation isotopes and snowmelt isotopes (due to the lack of snow elusion fractionation; Ala-aho
430 et al., 2017), the incorrect isotopic composition in groundwater, or the reduced applicability of degree-
431 day model for mountainous areas in Europe. Nitrate Such simulation deviation due to the uncertainty
432 in data and boundary initialisation is often reported in previous calibration (Smith et al., 2021).

433 In general, the model produces comparable performances to existing nitrogen modelling at catchment
434 (Wu et al., 2022, 2025b; Yang et al., 2018) and continental scales (Jones et al., 2023; Mikayilov et al.,
435 2015). However, nitrate simulations also failed to capture the observations at three sites. However,
436 though as is shown in Figure 4, these sites all have relatively low levels of NO₃-N concentrations. Such
437 low average values can easily trigger the degradation of their KGE statistic—as one of the sub-
438 components of KGE is highly sensitive to the mean deviation, though the absolute deviation remained
439 low (Figure 4). Given the good performance at the remaining sites, Table 2). Overall, we concluded
440 that EcoTWIN has the good capacity to reproduce in-stream components for a wide range of
441 catchments and for relatively long periods.

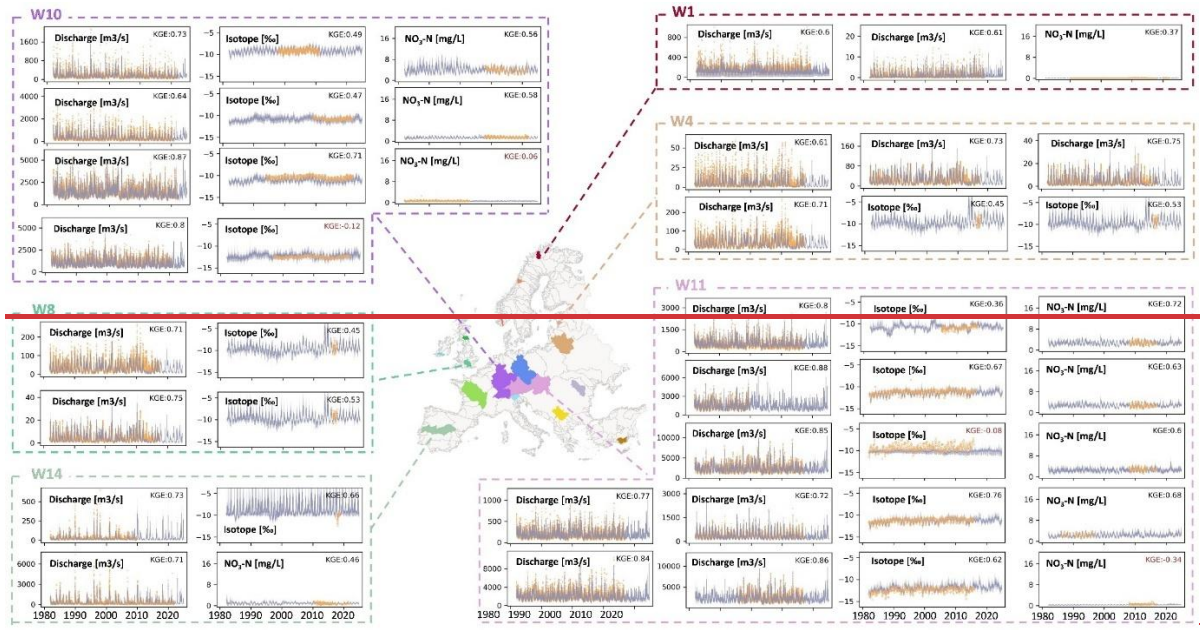
442



443

444 **Figure 3. The simulation5 Validation performance of discharge, in-stream isotope, and in-stream**
445 **NO₃-N.**

446



447

448

449

450

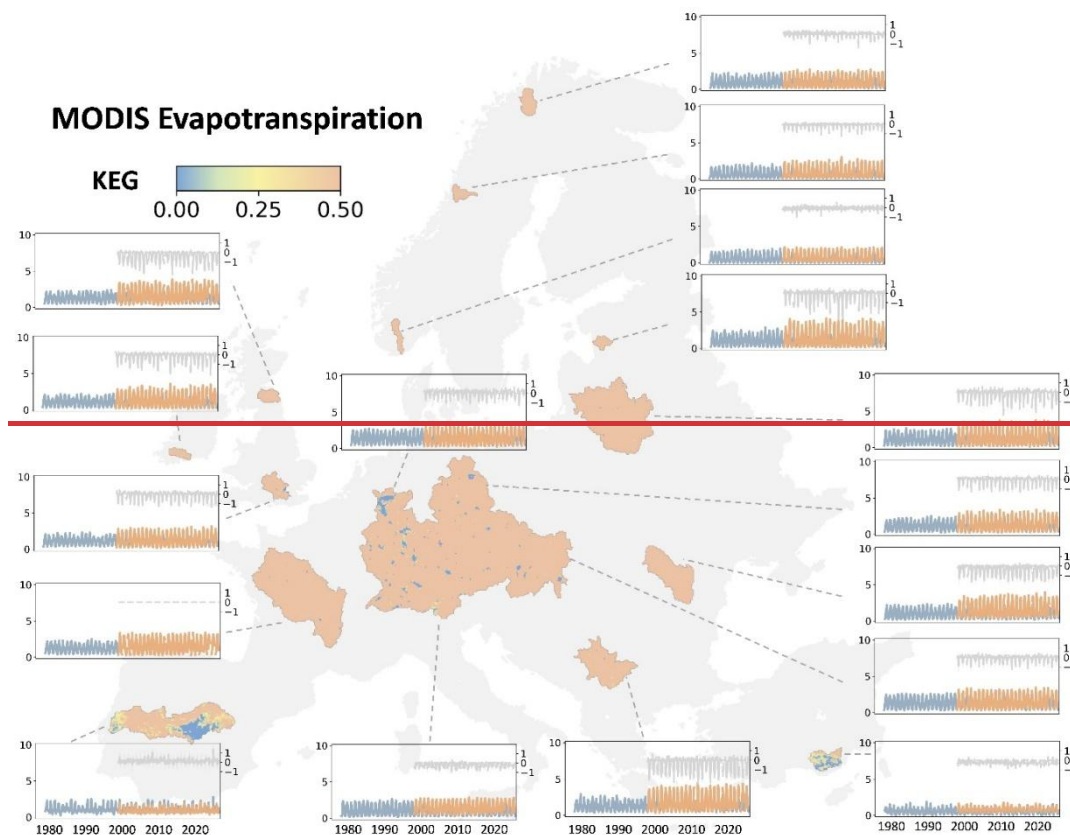
Figure 4. The simulated (blue) and observed (orange) time series of discharge, isotopes, and $\text{NO}_3\text{-N}$ at representative gauges. Note that the sites with relatively poor performance ($\text{KGE} < 0.2$) were particularly shown for model diagnosis.

451

452 4.2 Validation

453 Apart from the variables used for calibration, three internal states and fluxes are also compared with
 454 remote sensing products. First, the sum of soil evaporation, channel evaporation, and transpiration
 455 was compared to MODIS evapotranspiration in each grid cell. The results in Figure 5 shows a general
 456 good fit between simulation and observation with r^2 above 0.5 in most regions. From the subplots in
 457 Figure 5, we can see that the seasonality and magnitude of evapotranspiration were well captured
 458 though the peaks in summer were slightly underestimated.

459



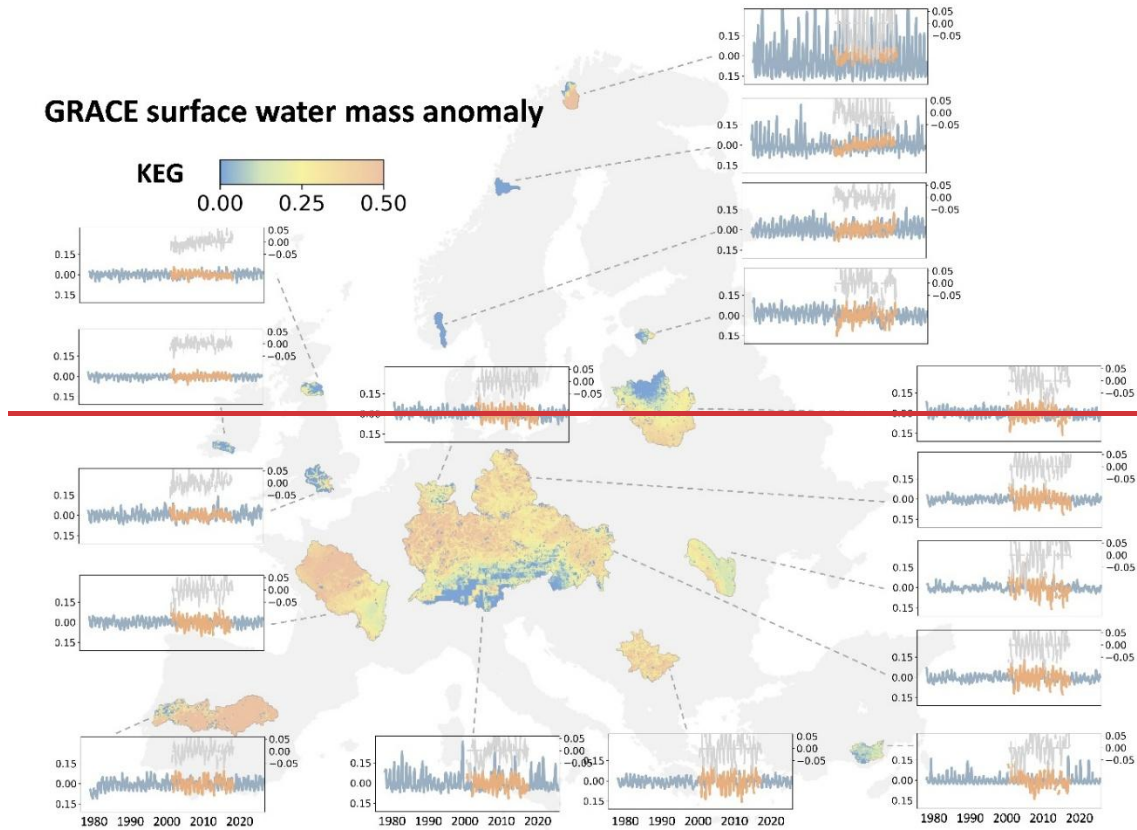
460

461 ~~Figure 5. The grid-to-grid comparison between simulated evapotranspiration and MODIS~~
 462 ~~evapotranspiration. The time series show the monthly mean of simulated (blue) and observed (orange)~~
 463 ~~values, as well as the deviations (grey).~~

464

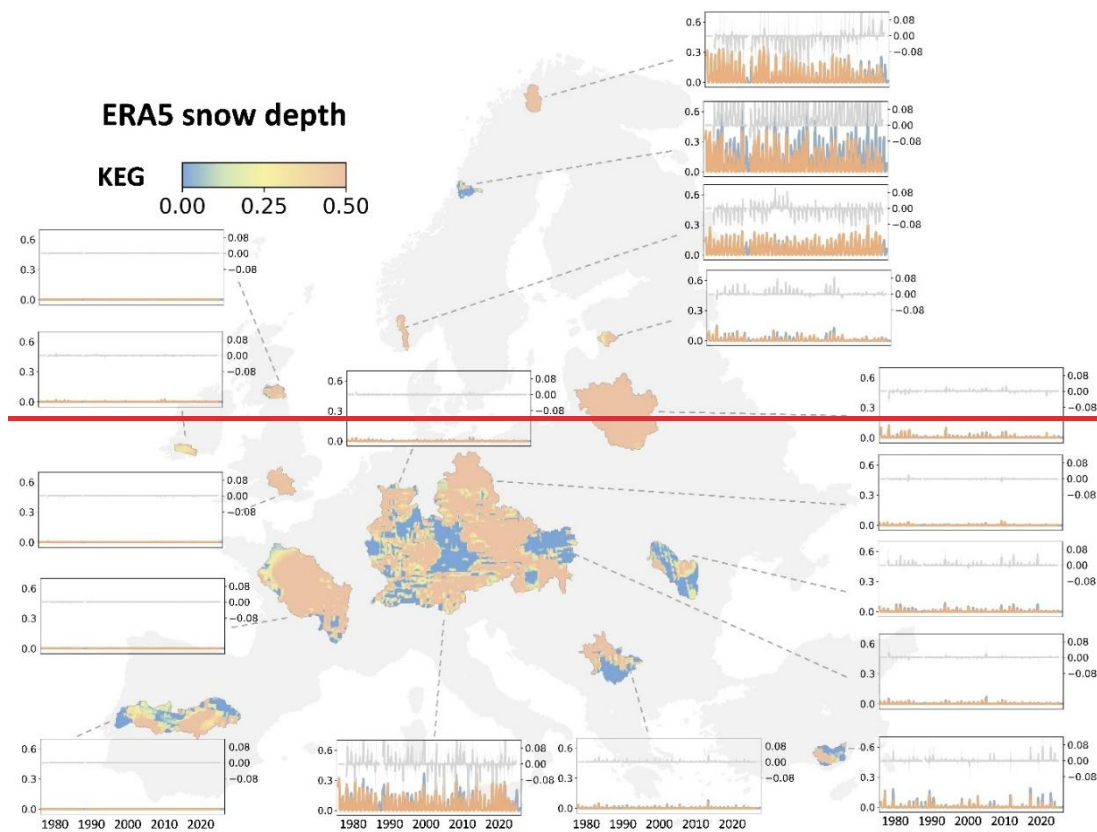
465 Then, the water storage anomaly was compared to the anomaly of simulated surface storage, i.e., the
 466 sum of canopy storage, snow, soil water storages, and ~~vadoseunsaturated~~ storage. The grid-to-grid
 467 comparison in Figure 6 shows a general good fit in most regions with r^2 close to or above 0.5. However,
 468 more degradation was found compared to the performance in evapotranspiration, especially in
 469 coastal regions. For instance, GRACE exhibited considerably increasing trends in water storage
 470 between 2005 to 2015 in two Nordic catchments (W2 and W3), yet our simulations only showed a

471 moderate increasing trend. Similar degraded performance was found in the coastal catchments (e.g.,
 472 three British catchments W6-8 in UK), though the magnitudes of simulation and observations fit well.
 473 This is possibly attributed to the coarse resolution of GRACE which additionally considered the storage
 474 mass from ocean in coastal region yet not included in this terrestrial-explicit modelling.



475
 476 ~~Figure 6. The grid to grid comparison between simulated water storage anomaly and GRACE surface~~
 477 ~~water mass anomaly. The time series show the monthly mean of simulated (blue) and observed~~
 478 ~~(orange) values, as well as the deviations (grey).~~

479
 480 Finally, the simulated snow depth was compared to the [daily snow depth in ERA5 reanalysis products-](#)
 481 [\(ERA5 post-processed daily statistics on single levels; 10.24381/cds.4991cf48\)](#). Results in Figure 7
 482 show a good agreement between simulations and [observations ERA5 records](#) in most regions with $r^2 >$
 483 0.5 , though degradation was found in a few catchments. Note that, the poor performances were
 484 generally found in catchments with limited snow accumulation, e.g., W14-17 in subplots in Figure 7.
 485 In the other words, the absolute deviation was relatively limited for snow depth simulation.



486

487 ~~Figure 7. The grid to grid comparison between simulated snow depth and ERA5 snow depth. The time~~
 488 ~~series show the monthly mean of simulated (blue) and observed (orange) values, as well as the~~
 489 ~~deviations (grey).~~

490

491 **4.3 Simulated water Water age simulation and its link to water quality**

492 Like many existing distributed hydrological and water quality models (e.g., SWAT, mHM, Ech₂O-iso,
 493 HYPE etc.), EcoTWIN can provide estimation of the main ecohydrological fluxes at high spatial and
 494 temporal resolutions, including canopy interception, snow melt-accumulation, infiltration, percolation
 495 through soil layers, groundwater recharge, and lateral flux routing at different horizontal phrases.
 496 Among these variables, a unique trait of EcoTWIN lies in its capacity to track water fluxes via isotopes,
 497 thus being able to provide a consistent estimate of water age and travel times. Therefore, in Figure 8,
 498 both variables are shown as the long-term average from 1982 to 2024 for soil profile and stream water.

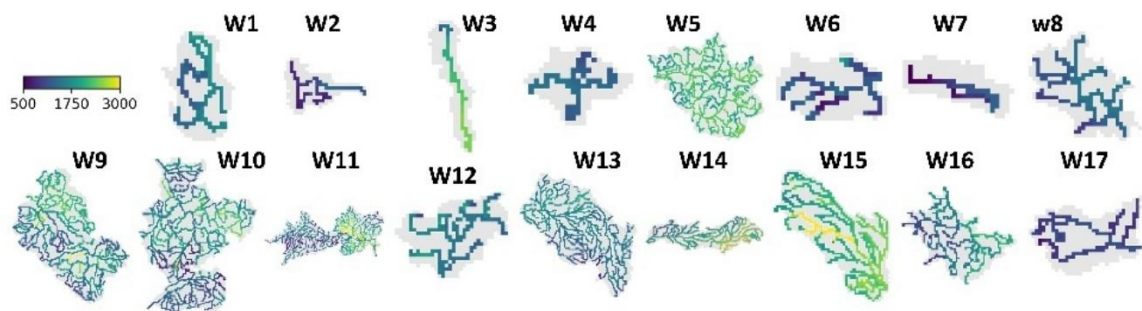
499 Generally, the magnitudes of water ages follow the geographic and climatic gradients, with younger
 500 water found in catchments with higher annual precipitation inputs. Those regions locate in the north-
 501 west coast of Europe (Figure 2), particularly for Nordic catchments where lower temperature and net
 502 radiation further limit the level of potential evapotranspiration, leading to larger percolation to deeper
 503 soil layers and groundwater. Such high turnover rates of water in these catchments (W1, W2, W3, W4,
 504 W5, and W8) are also demonstrated as the simulated travel time in soil profile with average values
 505 remaining below 500 days.

506 A similar pattern was also found in mountainous regions with higher precipitation and lower potential
507 evapotranspiration compared to lowland areas. Two clear examples are W12 and W17 located in the
508 Alps and the Taurus Mountains where water ages and travel time remained below 500 days (Figure
509 2). In specific wet periods, the water ages and travel time can be reduced to just days, suggesting the
510 rapid response of saturated hydrological systems (e.g., the wet year 1999 in Europe in Figure S1-S3).
511 In contrast, the lowlands in central-west Europe showed much slower turnover rates, with the mean
512 water ages reaching almost 10 years in some specific regions. A few examples could be found in the
513 three major representative catchments in Central Europe – Elbe, Rhine, and Danube (W9-11). Such
514 old water ages and long travel time are further exacerbated during dry years (e.g., 2004, a drought
515 year for much of Europe shown in Figure S1-3).

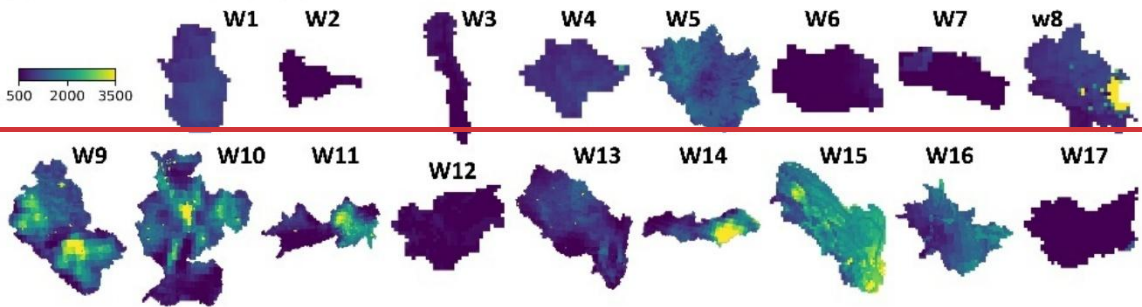
516 Note that though water ages and travel time share similar magnitudes and spatial patterns. It is partly
517 attributed to the fact that the travel time in the conceptualised storages increases exponentially in a
518 sequential order. Taking the Rhine as an example, the average travel time in top soil layer, median soil
519 layer, deep soil layer are 65, 225, 1291 days, respectively. Such a depth-dependence profile makes the
520 overall ages/travel time follow the magnitude of bottom layer and leads to similarity between water
521 ages and travel time. However, large discrepancies are possible between the two indices if a shallow
522 lower boundary is adopted.

523

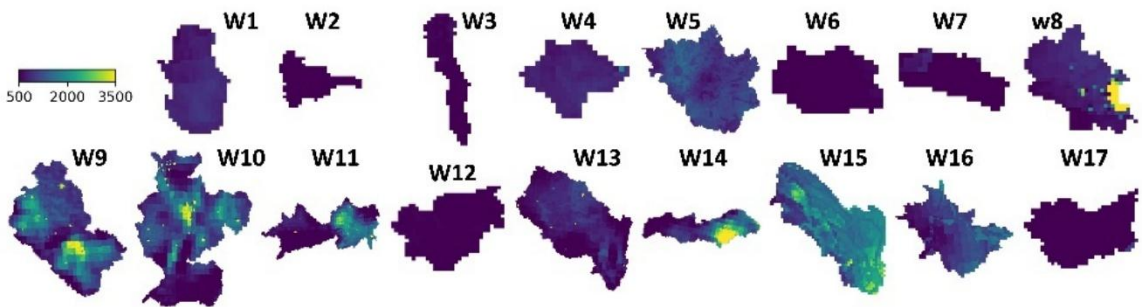
(a) Stream water age [days]



(b) Soil water ages [days]



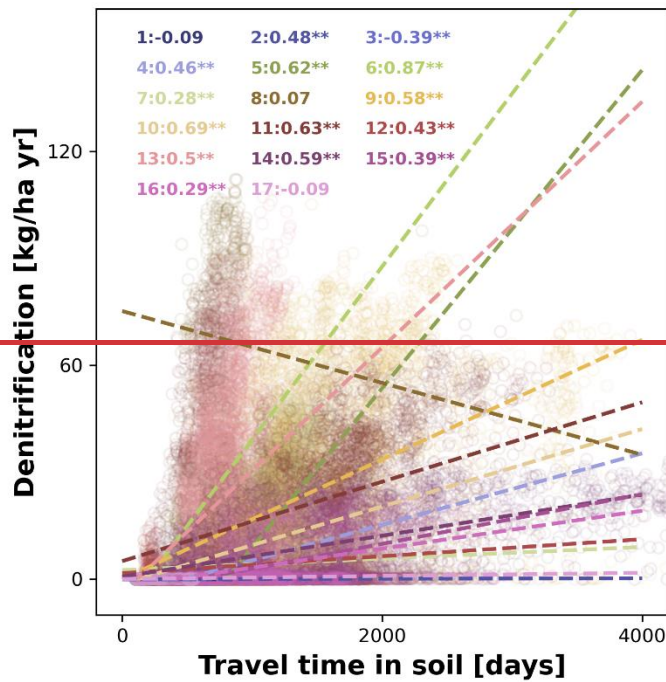
(c) Travel time in soils [days]



524

525 Figure 8. The simulated long term average (1982-2024) of water age and travel time in channel and
526 soil profile. Water ages represent the time since water enters the catchments as precipitation, while
527 travel times depict the residence time of water within the specific storage.

528



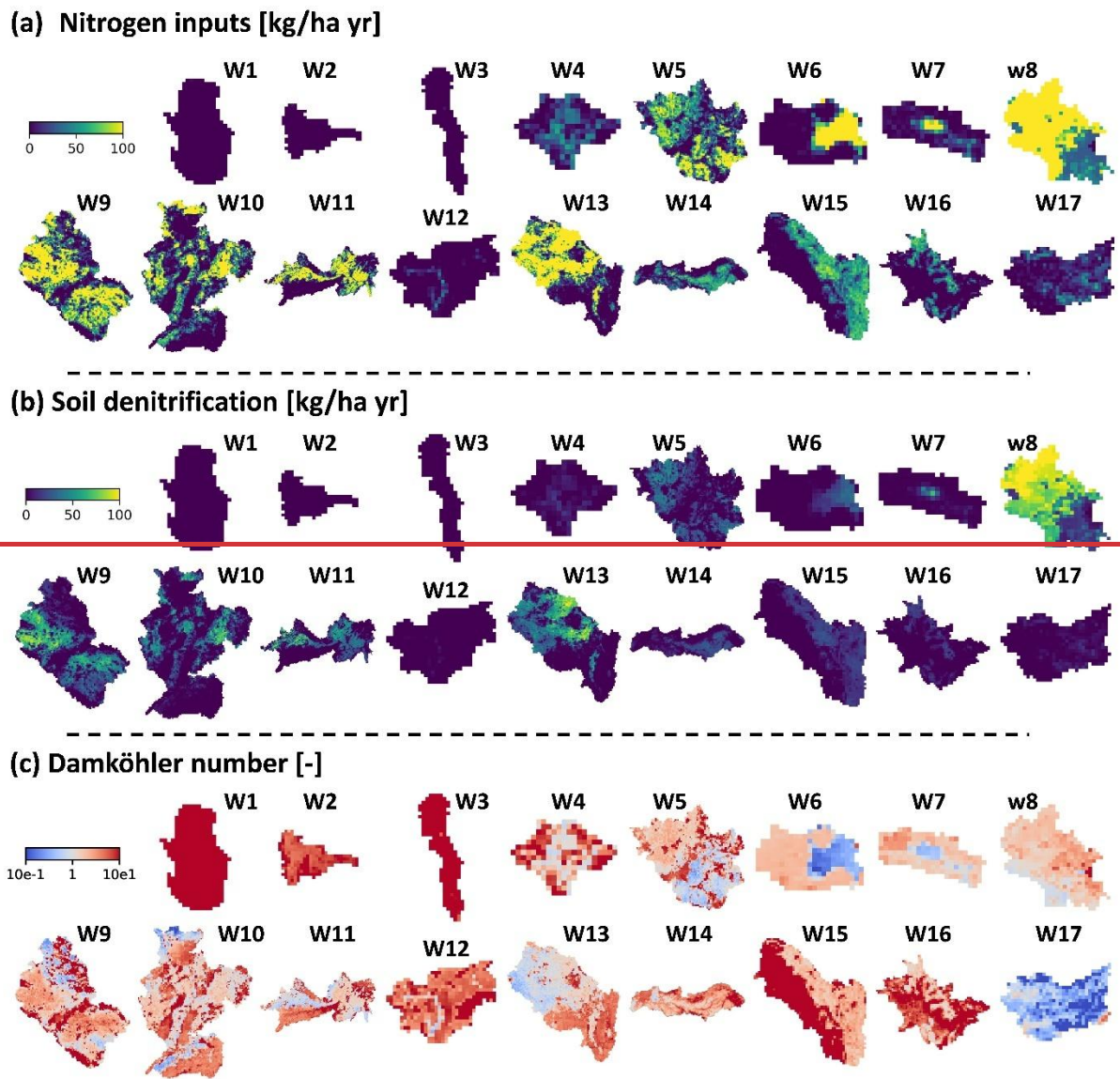
529

530 ~~Figure 9. The correlations between travel time and annual denitrification. The text depicts the~~
 531 ~~spearman correlation coefficients and p values (* = less than 0.05, ** = less than 0.01) in each~~
 532 ~~catchment.~~

533

534 The estimation of travel time and water ages further provides opportunities to link hydrology and
 535 water quality processes in the modelling framework. The simplest and most intuitive way is to
 536 compare travel times and simulated biogeochemical process kinetics. Taking denitrification as an
 537 example, we applied linear regression and Spearman’s correlation test to investigate the potential
 538 correlation between travel time of soil water and denitrification rates. The results in Figure 9 showed
 539 the strong positive correlations in most agricultural-dominated catchments (W5, W5, W6, W8, W9,
 540 W11) yet only weak or no correlation in remaining pristine watersheds. This suggests that travel time
 541 might be a key control on soil nitrogen removal in European croplands.

542 More insights can be gained via examination of the Damköhler Number, which quantifies the ratio
 543 between timescales of chemicalsolute transport and biogeochemical transformation. Here in our
 544 modelling framework, it can be calculated as the ratio between the travel time of soil water and the
 545 time for all soil NO₃-N storage to be removed under the simulated denitrification rates. Damköhler
 546 numbers <1 mean that soil water nitrogen cannot be fully removed during time of residence,
 547 indicating the dominance of transport over removal processes and the potential of nitrogen leaching.
 548 As shown in Figure 10c, the long-term averages of Damköhler number remain below 1 in most
 549 croplands, supporting the conclusion from the linear regression (travel time is a major limiting factor
 550 on soil nitrogen removal). Via the spatial- and temporal-explicit estimation of Damköhler number,
 551 EcoTWIN provides the opportunity to bridge the catchment hydrological and water quality with travel
 552 time.



554

555 ~~Figure 10. The simulated long term average (1982-2024) of nitrogen inputs, soil denitrification, and~~
 556 ~~Damköhler number.~~

557

558 **5 Discussion**

559 **5.1 Structural and Functional Merits of EcoTWIN**

560 As a new tracer-aided ecohydrological model, EcoTWIN has a novel advantages compared to previous
 561 models. In this section, we briefly introduced the merits in model structure, applicability, and insights
 562 from tracer-aided simulation.

563 **5.1.1 Integrated C++ framework**

564 Applications of large-scale modelling have been increasingly popular due to the accelerating
 565 development of observation networks and availability of remote sensed data. However, it increases

566 severely increases the computational burden of ecohydrological modelling. Especially for fully
567 distributed models, increasing size of the model domain can lead to exponential increase in
568 computation demands. In this context, an integrated C++ framework in C++ can significantly accelerate
569 the modelling tasks, as all computation can be conducted within memory thereby avoiding the
570 additional input/output overhead associated with disk-based operations in loosely coupled model
571 chains (e.g., ECH₂O-iso-nitrate; Yang et al., 2024). A standard test was not performed, but based on
572 our modelling experience in the same catchment with different models, the speed of EcoTWIN (~5
573 seconds for a simulation with 285 grid cells and 30 years at daily timestep) is close to the water quality
574 model mHM-Nitrate (~5 seconds yet without isotopic simulations; Wu et al., 2022) and easily
575 outperforms ECH₂O-iso-nitrate (7 minutes; Wu et al., 2025b).

576 **5.1.2 Selective disassembly structure**

577 EcoTWIN incorporates a wide range of ecohydrological processes from canopy to groundwater, which
578 not only include natural processes but also anthropogenic activities like irrigation. Land managements
579 can also be represented by dynamicaldynamic parametrisation, thus enabling EcoTWIN to function as
580 a learning tool to investigate the impacts of changes in anthropogenic management over natural
581 ecosystems; for instance, the land use distribution was updated every 10 years in our test examples
582 to reflect the moderate increases in afforestation in the past 45 years in Europe. More importantly,
583 unlike hard coded process representations/equations in most ecohydrological models, EcoTWIN has
584 a selective disassembly structure, which provides alternative conceptualisations for several important
585 hydrological processes (canopy interception, percolation, groundwater recharge, as well as three
586 pedotransfer functions for initialising soil properties). Modellers can benefit from such flexible model
587 structurestructures by either selecting process representations best suited to field knowledge or data
588 prior to calibration, or integrating module selection into the calibration thus enabling simultaneous
589 optimisation of model structure and corresponding parameters. The latter aspect, i.e., the
590 optimisation of model structure, can be realised together with the recently developed optimisation
591 algorithm DREAM_(LOAX) that aims to identify the deficits in model structure during calibration (Wu et
592 al., 2025a).

593 **5.1.3 Transferability to contrasting geographic and climatic contexts**

594 To thoroughly test the applicability of EcoTWIN, 17 catchments with different climatic and
595 geographical contexts were selected for calibration and validation, spanning over most biomes in
596 Europe, from snow-dominated watersheds in Nordic or alpine regions, to agricultural-influenced
597 lowlands catchments, and Mediterranean ecosystems (Figure 1 and Table 1). Through multi-criteria
598 calibration against three objectives at multiple sites, the model successfully reproduced the
599 seasonality and peaks of discharge, in-stream isotopes, and NO₃-N concentrations in most catchments.
600 Such performance is comparable or better than the previous model benchmarks at similar scales
601 (Bajracharya et al., 2023; Mikayilov et al., 2015; Rakovec et al., 2016, 2019). Note that the
602 concentration of NO₃-N was used for calibration, whose accurate simulation is more difficult than NO₃-
603 N loads given the naturally good performance in discharge. In the other words, hydrological simulation

604 is often the least problematic part in integrated water quality modelling, as it is mostly dominated by
605 natural catchment properties while nitrogen cycling is more interfered by anthropogenic
606 managements (e.g., fertilization and irrigation) (Wu et al., 2025b). Additionally, the simulated internal
607 fluxes were also compared to three reanalysis products in hydrological simulations, corresponding to
608 the key fluxes or storage states in hydrological cycling (snow melt-accumulation, evapotranspiration,
609 and water storage). The results show that constrained by isotopes, EcoTWIN was able to reproduce
610 comparable hydrological modelling results to the remote sensing observations without direct
611 calibration regarding magnitudes, spatial patterns, and temporal dynamics. The only degraded
612 performance was found in GRACE surface mass anomaly in coastal regions. There are two potential
613 reasons: (i) the coarse resolution of GRACE might account for mass shifts in both ocean and land, yet
614 EcoTWIN only produces mass anomaly in terrestrial systems; (ii) bidirectional fluxes across the land-
615 ocean interface might drive key changes in coastal systems, which is not considered in current version
616 of EcoTWIN. Nonetheless, given the relatively good agreement with most available observations, we
617 conclude that EcoTWIN is applicable across a range of terrestrial ecosystems from boreal to temperate
618 and subtropical climate.

619 **5.1.4 Bridging hydrology and water quality with water ages**

620 Further to the inference of hydrological and nitrogen processes that is also available in other
621 distributed water quality models (Wellen et al., 2015), ~~one~~ a unique trait of EcoTWIN lies in its capacity
622 to track water fluxes and ages with stable water isotopes. As a tracer-aided model, EcoTWIN not only
623 simulates the celerity of catchment response, but tracks the velocity of water via different flow paths.
624 The importance of delineating flow paths within catchments has long been recognized by hydrologists,
625 and has motivated the development of many indices to describe the movement of water molecule at
626 catchment-scale and estimate associated timescales (Sprenger et al., 2019). A few examples are water
627 ages, transient time distribution, and young water fractions (Benettin et al., 2015; Hrachowitz et al.,
628 2013; Jasechko et al., 2016). However, those indices are mainly calculated in a lumped manner where
629 different flow paths in the catchment are characterised as a black box, thus characterising the overall
630 input-output dynamics yet potentially omitting important spatio-temporal variability of hydrological
631 boundary conditions. Instead, EcoTWIN, benefiting from the gridded-based structure, can utilise the
632 increasingly available spatial information (e.g., gridded remote sensing datasets) thus characterising
633 the water ages and travel time in a spatially-explicit manner. Note that simulations of water age/travel
634 time, like other ecohydrological processes, are sensitive to spatial resolution. The coarse resolution
635 used for large catchments (e.g., 5 km in this study) may obscure the sub-grid heterogeneity. For
636 instance, local hydrological hotspots characterized by short travel times and young water ages can be
637 damped or averaged out at coarser resolutions, as reported in modelling studies using ECH2O-iso
638 (Smith et al., 2021; Yang et al., 2023b). However, this limitation can be mitigated by increasing spatial
639 resolution, and it does not undermine the utility of EcoTWIN for water-tracking.

640 Compared to water age which quantifies the age of water within the overall system, travel time,
641 accounting for the water age within a specific storage, is more important in understanding the links
642 between hydrological and nutrient cycles. Such an index, also known as transienttransit time or

643 exposure time, forms one of the ~~bases for~~ fundamental components of water quality modelling.
644 Therefore, the travel time estimated by EcoTWIN has potential to improve the simulation of
645 biogeochemical transformations in water quality models interfaced with simplified hydrological
646 modules (e.g., MONERIS; Bonchkovskyi & Osadcha, 2024). Moreover, travel time can be used as a
647 proxy to bridge hydrological processes and biogeochemical transformations. Here we presented a
648 simple framework to calculate the Damköhler Number for denitrification. By using the simulated
649 travel time and reaction timescale (i.e., the time for full removal of nitrogen storage under current
650 denitrification rates), estimation of Damköhler Number was achieved in a spatially- and temporally-
651 explicit manner (Figure 9), which can highlight where and when soil nitrogen removal is constrained
652 by the limited exposure time in the catchment. Such high-resolution information is unique, as the use
653 of this index has been largely restricted to steady-state groundwater systems or riparian/hyporheic
654 zones due to the difficulty in quantifying processing time and residence time at larger scales (Ocampo
655 et al., 2006; Wu et al., 2022).

656

657 **5.2 Limitations and roadmap for future development**

658 Despite these ~~unique traits~~ advances, EcoTWIN has limitations. In this section, the uncertainties in
659 model structure and conceptualisation are introduced, as well as the potential roadmaps for future
660 developments.

661 **5.2.1 Potential towards physics-based conceptualisation of groundwater**

662 Groundwater in EcoTWIN is characterised as ~~a single-layer storage~~ two conceptual storages linking
663 with adjacent upstream and downstream storages following the topographic gradients. Such
664 conceptualisation, although ~~it~~ has been widely employed in hydrological models (e.g., SWAT, mHM,
665 EcH₂O, STARR, etc.), does not align with the physical mechanisms of groundwater routing, as
666 groundwater flow direction follows the hydraulic gradients which may not entirely coincide with
667 topographic gradients (Condon et al., 2021). Such simplified routing has less effect in large catchments
668 with clear topographic gradients (e.g., Rhine starting from Alps to North plain), yet might cause biased
669 estimation in water mass balance for flatter headwater catchments (Yang et al., 2025). Therefore, we
670 plan to further incorporate an additional groundwater module to realise physics-based routing
671 following ~~the~~ Darcy's Law in future.

672 **5.2.2 Revisiting mixing strategies**

673 Mixing strategy is a key component in water quality or tracer models describing the flux-storage
674 behaviours along specific flow paths. There has long been a debate on different mixing assumptions
675 and theories. A typical example is the two-water-world hypothesis, where water storage in the soil
676 profile is differentiated into a tightly-bound pool and a mobile-water pool (McDonnell, 2014). Such
677 conceptualisation is close to the definition of soil matrix flow and preferential flow: the existence of
678 free-flowing preferential flow will bypass the soil matrix vertically and accelerate the lateral drainage
679 via direct connection with channel network (Hrachowitz et al., 2013; Sprenger et al., 2019). However,

680 a complete mixing strategy is often regarded as a reasonable first approximation in many situations
681 and is used in most water quality and tracer models (Jung et al., 2025). This is not only attributed to
682 its computational simplicity, but also the difficulty to conceptualise in conceptualising preferential flow
683 in an evidenced-based manner. In the other words, even with the recognition of preferential flow, its
684 calculation is often hindered by the subsurface heterogeneity in soils and bedrock; a good visualisation
685 is given in Figure 7 in Sprenger et al., (2019). Alternatively, partial mixing has been developed for
686 ecohydrological models (e.g., Hrachowitz et al., 2013), which could be added as a complementary
687 mixing strategy in EcoTWIN. However, as benchmarked in Hrachowitz et al., (2013), the partial mixing
688 brings only moderate improvements in simulations yet introduces can introduce challenges to model
689 spin-up (the increasing instability of storage ages due to the exchange between bypass and storage
690 compartment). Moreover, the realisation of partial mixing, like preferential flow, relies on additional
691 parameters to describe the timing and extent of mixing thus introducing additional parametric
692 uncertainty. Therefore, we recommend a rigorous evaluation of the necessity of partial
693 mixing before any application.

694 **5.2.3 Complementing the in-stream biogeochemical processes**

695 Transformation is as crucial as transport in inland-water nitrogen cycling (Wang et al., 2024). In the
696 current version of EcoTWIN, denitrification is the only in-stream process of nitrogen retention loss.
697 However, recent studies have shown that other processes are involved which may be important for
698 aquatic nitrogen cycling. An example originates from Wang et al., (2024), where global inland-water
699 modelling shows that in-stream denitrification only accounts for a minor fraction of NO₃-N removal
700 compared to biological uptake. Though their modelling considers lakes and reservoirs where
701 primary production of benthic plants and algae is usually greater than that in rivers, the in-stream
702 assimilation might still play a significant role, particularly, in slow-flowing river systems. This is
703 supported by a recent modelling study that estimated nitrogen retention at 15-min interval based on
704 high-frequency NO₃-N data (Yang et al., 2023a). Therefore, we plan to further compliment EcoTWIN
705 with in-stream assimilation conceptualisation, as well as other potentially important riverine
706 processes (e.g., nitrogen burial in sediments; Akbarzadeh et al., 2019).

707 **5.2.4 Integrated calibration framework to embrace equifinality**

708 Strictly speaking, equifinality is not specifically linked to EcoTWIN, but remains a universal problem for
709 calibration or parameter tuning for almost all ecohydrological models. It is reflected in multiple
710 parameters sets yielding similarly good model performance, thus increasing the uncertainty in process
711 inference. The extent of equifinality is primarily controlled by the magnitude of parameters and
712 observation/objectives (Wu et al., 2025c). Unfortunately, conceptualisations across diverse process
713 domains (e.g. for hydrology, isotopes and N-cycling) in EcoTWIN also lead to a relatively large number
714 of parameters. Such risk in equifinality can be potentially constrained via sensitivity analysis, but can
715 still remain an issue given the ubiquitous epistemic uncertainty in data and model structure (Beven,
716 2006, 2015). Alternatively, the recently developed calibration algorithm DREAM_(LoAX) provides an
717 opportunity to embrace equifinality by tuning parameters based on the limits-of-acceptability theory

718 under the equifinality thesis (Wu et al., 2025a). The integrated modelling framework of EcoTWIN and
719 DREAM_(LoAX) can potentially increase the robustness of model calibration and inference.

720

721 **6 Conclusions**

722 Uncertainty is a central concern in ecohydrological modelling, as models are not only used for
723 prediction of specific variables, but also for process inference (backtracking internal processes from
724 available observations) that are inherently embedded within considerable uncertainty. Stable water
725 isotopes can help effectively constrain hydrological fluxes due to their conservative nature, motivating
726 the increased development of tracer-aided models. However, few attempts have been made to
727 incorporate a tracer-aided hydrological framework into water quality models.

728 Therefore, we ~~introduce~~introduced EcoTWIN, a fully distributed tracer-aided **ecohydrological** model
729 that **tracks water, isotopic, and nutrient** fluxes simultaneously in an integrated ~~C++~~C++-based
730 framework. To thoroughly validate the model, 17 large European catchments were selected with a
731 wide range of geographic and climatic gradients (from snow-dominated watersheds in Nordic or alpine
732 regions, to agricultural-influenced lowlands catchments, and ~~mediterranean~~Mediterranean
733 ecosystems). The model was calibrated against long-term observations of discharge, in-stream
734 isotopes, and NO₃-N concentrations during 1980-2024 in each of the 17 catchments. Additionally,
735 uncalibrated internal states and fluxes were also compared with three remote sensing products (ERA5
736 snow depth, MODIS evapotranspiration, and GRACE surface water anomaly) to validate the credibility
737 of process inference.

738 The generally good agreements in both calibrated in-stream components and uncalibrated internal
739 flux-states demonstrated that EcoTWIN is a transferable, flexible prediction and learning tool for
740 process inference across biomes ranging from boreal to subtropical climate. Constrained by tracer
741 simulations, the model not only reproduces the celerity of hydrological systems, but also tracks the
742 velocity. Water ages and travel time are embedded in EcoTWIN to provides spatio-temporal-explicit
743 insights into *when, where, and how* water moves in the system. Such indices further provide the
744 opportunities to efficiently bridge hydrology and water quality at large catchment-scales. An example
745 was presented using the Damköhler Number to identify regions where denitrification was limited by
746 fast turnover rates of water.

747 Following this “proof of concept” we also see numerous areas where future developments can
748 improve the limitations in the 1.0 version of the model.

749

750 **Code and data availability**

751 The initial version (v1.0) of EcoTWIN is archived in <https://doi.org/10.5281/zenodo.16747633> (Wu et
752 al., 2025d). For further development please refer to GitHub repository: [https://github.com/songjun-
753 wu/EcoTWIN](https://github.com/songjun-wu/EcoTWIN). The geographic data were acquired from Catchment Characterisation and Modelling

754 database (CCM2, version 2.1). The climatic forcing was acquired from E-OBS database
755 (<https://www.ecad.eu/download/ensembles/ensembles.php>). The LAI were acquired from MODIS
756 database (<http://doi.org/10.5067/MODIS/MOD15A2H.006>). Long-term observation of discharge was
757 acquired from GRDC (<https://grdc.bafg.de/>); in-stream isotopic observations were available from
758 Wateriso database (<https://wateriso.utah.edu/waterisotopes/index.html>) and GNIR database
759 (<https://www.iaea.org/services/networks/gnir>); In-stream NO₃-N concentration were acquired from
760 global water quality database, GEMStat (<https://gemstat.org/>).

761

762 **Acknowledgements**

763 Tetzlaff's and Wu's contributions were partly funded through the WETSCAPES2.0 project (DFG
764 TRR410/1 2025) and the Einstein Research Unit "Climate and Water under Change" from the Einstein
765 Foundation Berlin and Berlin University Alliance (grant no. ERU-2020-609). Tetzlaff was also partly
766 funded through Leibniz Excellence project ISOSCALE and received funding from the
767 "Wasserressourcenpreis 2024" of the Rüdiger Kurt Bode-Foundation. This research was also
768 supported by the BMBF (funding code 033W034A), which supported the IGB stable isotope Laboratory.
769 Contributions from Soulsby were supported by Leibniz Association Germany in the project Wetland
770 Restoration in Peatlands.

771

772 **Author contribution**

773 Conceptualization: SW, DT, YZ, CS

774 Data curation: SW

775 Methodology: SW

776 Software: SW

777 Investigation: SW, DT, YZ, CS

778 Visualization: SW

779 Supervision: DT, CS

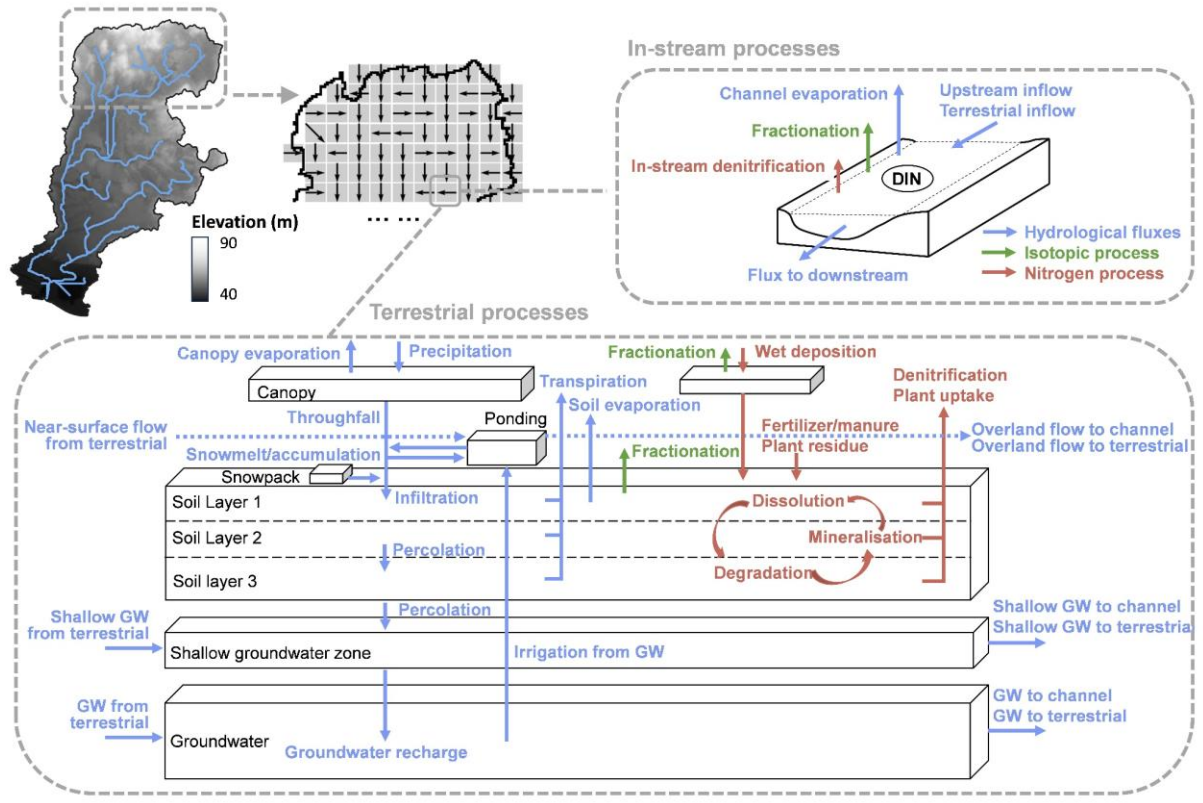
780 Writing (original draft preparation): SW

781 Writing (review and editing): SW, DT, YZ, CS

782

783

Figures

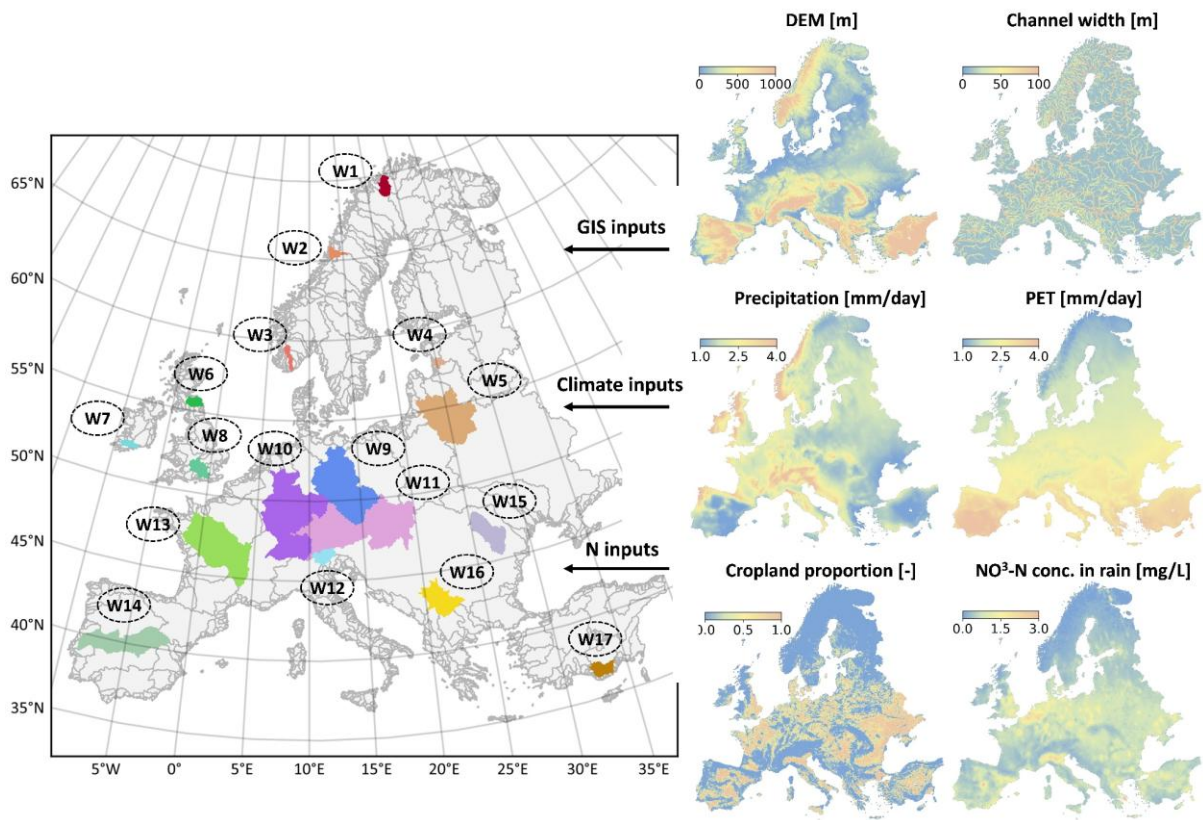


784

785 Figure 1. Model structure of EcoTWIN. As a distributed model, EcoTWIN disentangles the spatial
 786 domain into grid cells. In each grid cell, hydrological, isotopic, and nitrogen processes were simulated
 787 in canopy, snow, soils, shallow groundwater, groundwater, and channel.

788

789

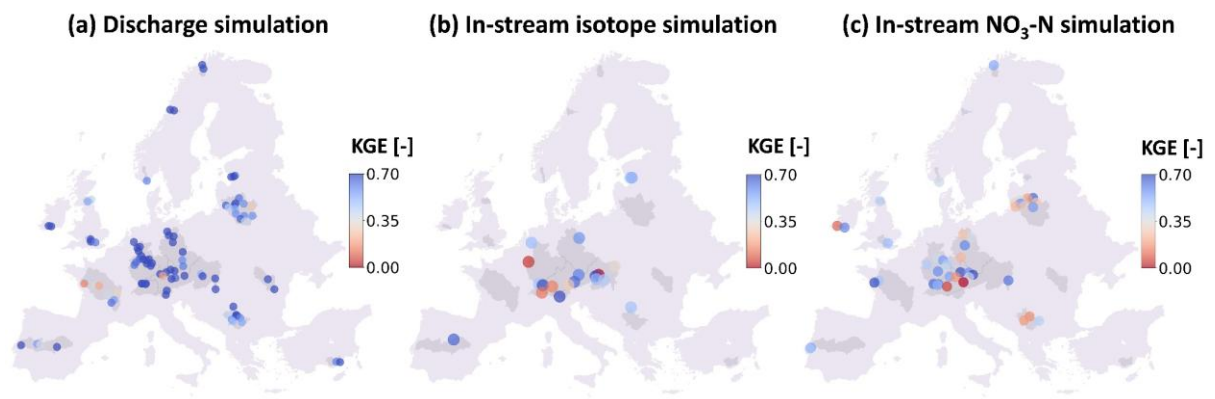


790

791 Figure 2. The selected catchments for model validation and an overview of key inputs.

792

793

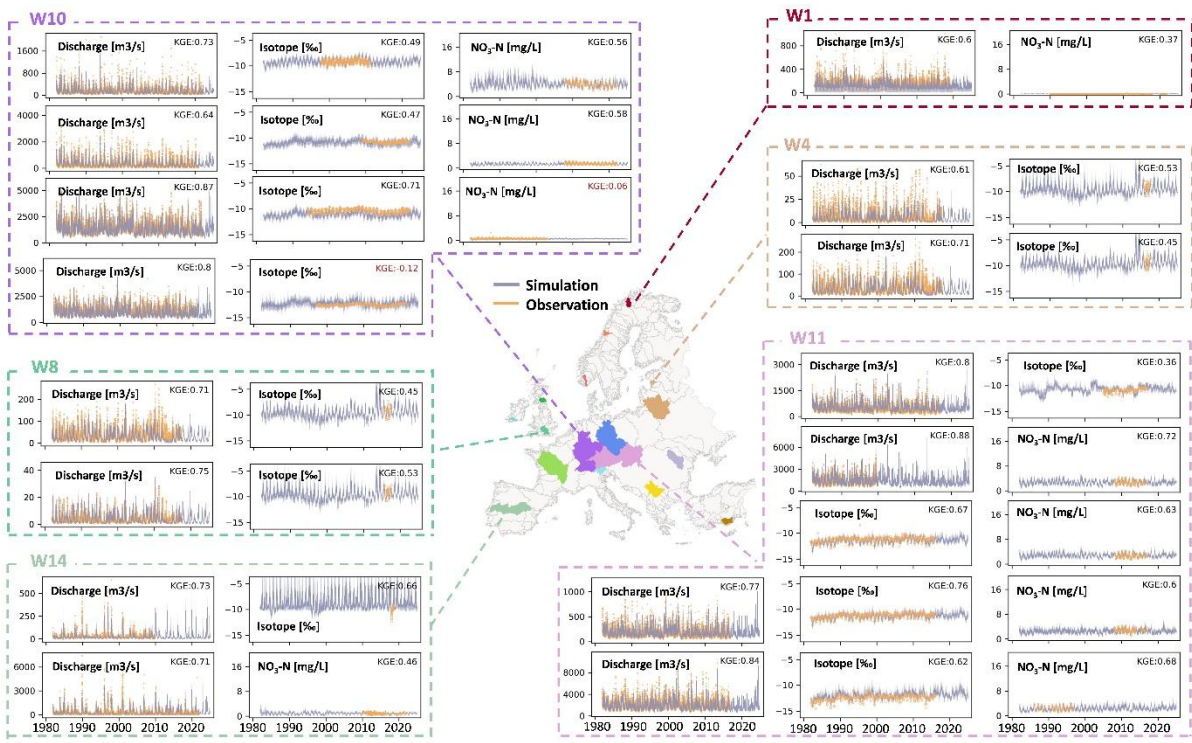


794

795

Figure 3. The simulation performance of discharge, in-stream isotope, and in-stream NO₃-N.

796



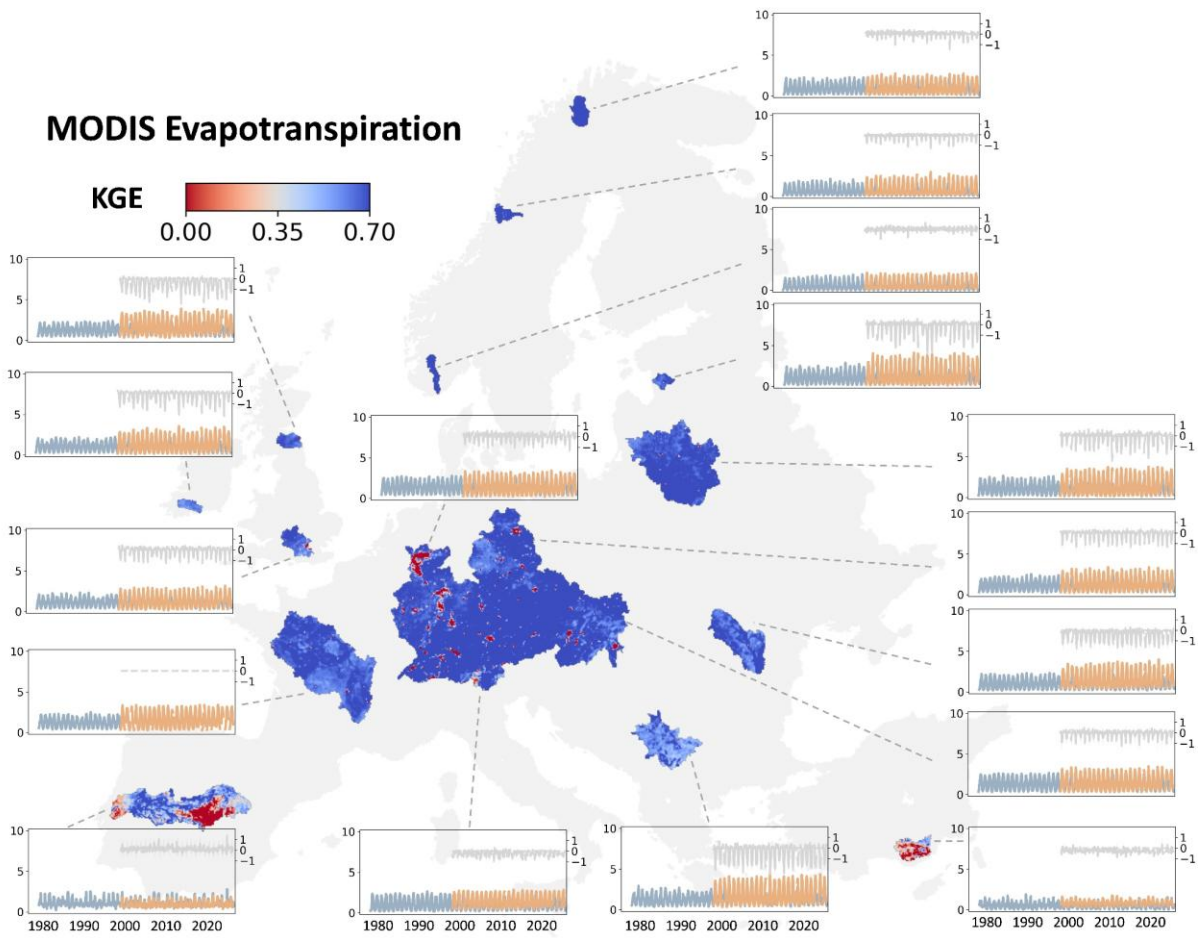
798

799

800

801

Figure 4. The simulated (blue) and observed (orange) time series of discharge, isotopes, and NO₃-N at representative gauges. Note that the sites with relatively poor performance (KGE < 0.2) were particularly shown for model diagnosis.

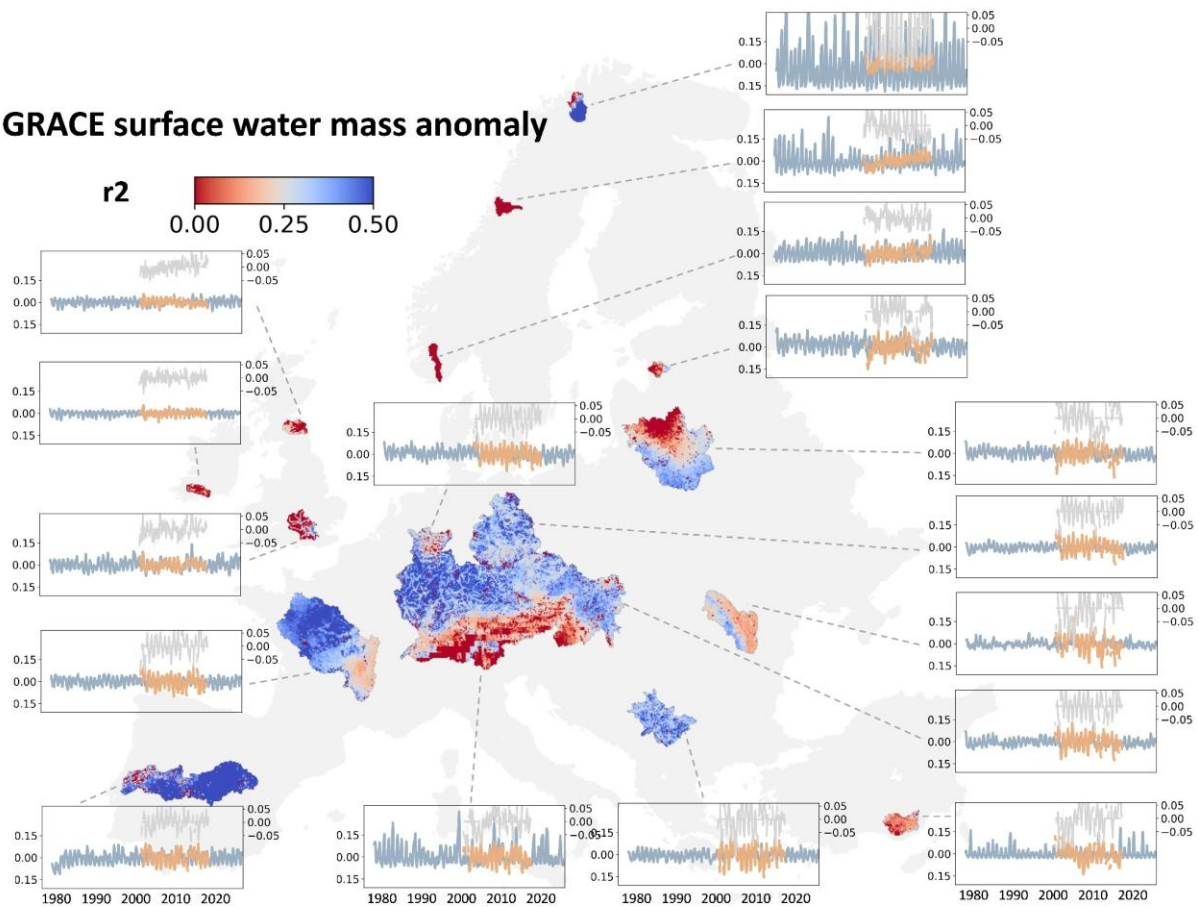


802

803 Figure 5. The grid-to-grid comparison between simulated evapotranspiration and MODIS
 804 evapotranspiration shown in KGE. The time series in inset subplots show the monthly dynamics of
 805 simulated (blue) and observed (orange) values averaged from all grid cells in the watershed, as well
 806 as their deviations (grey).

807

GRACE surface water mass anomaly

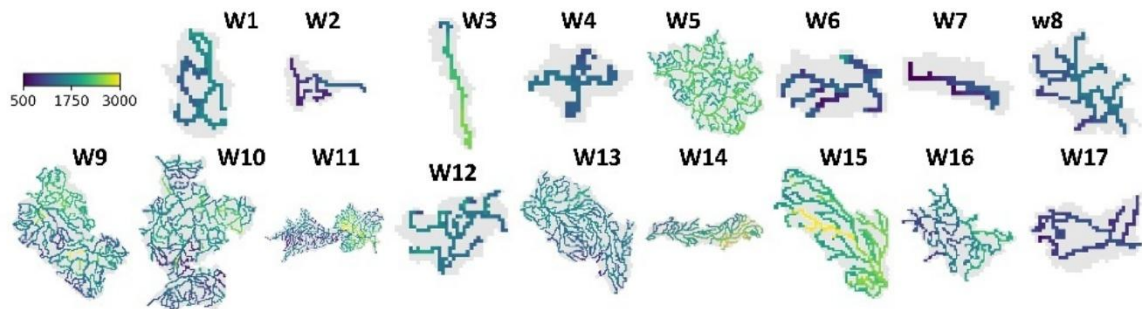


808

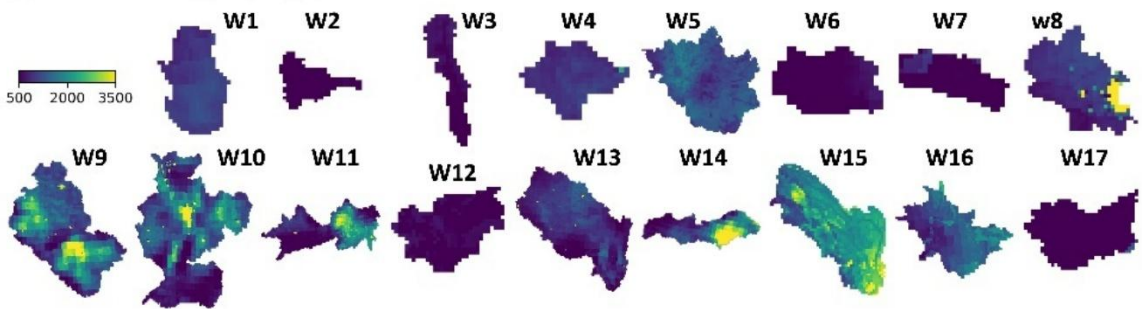
809 Figure 6. The grid-to-grid comparison between simulated water storage anomaly and GRACE surface
810 water mass anomaly. The time series show the monthly dynamics of simulated (blue) and observed
811 (orange) values averaged from all grid cells in the watershed, as well as their deviations (grey).

812

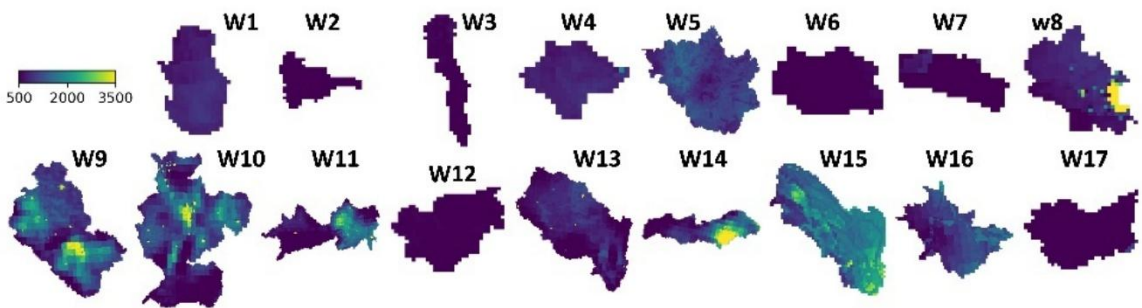
(a) Stream water age [days]



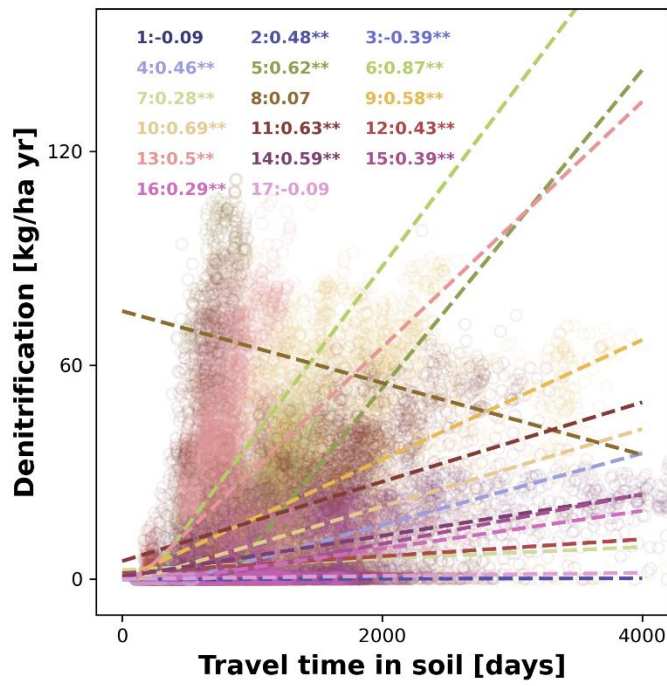
(b) Soil water ages [days]



(c) Travel time in soils [days]



820 Figure 8. The simulated long-term average (1982-2024) of water age and travel time in channel and
821 soil profile. Water ages represent the time since water enters the catchments as precipitation, while
822 travel times depict the residence time of water within the specific storage.

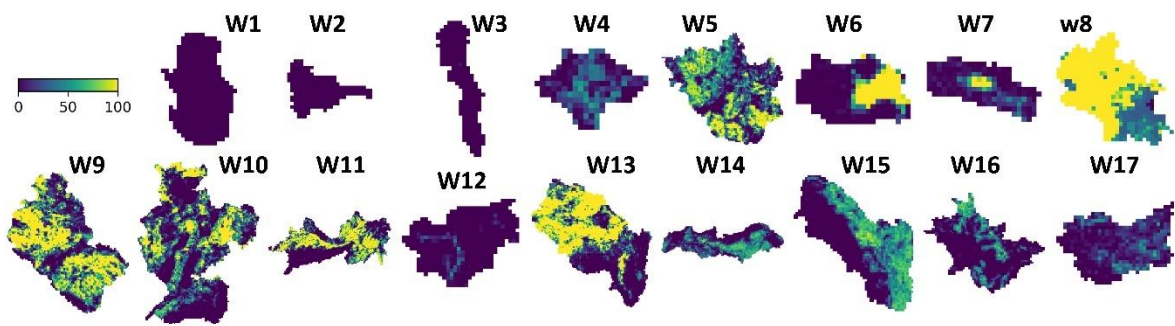


824

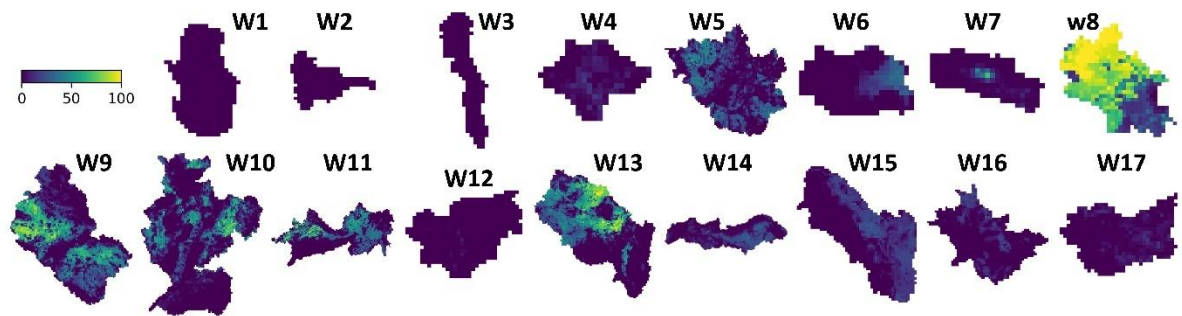
825 Figure 9. The correlations between travel time and annual denitrification. The text depicts the
 826 spearman correlation coefficients and p values (* = less than 0.05, ** = less than 0.01) in each
 827 catchment.

828

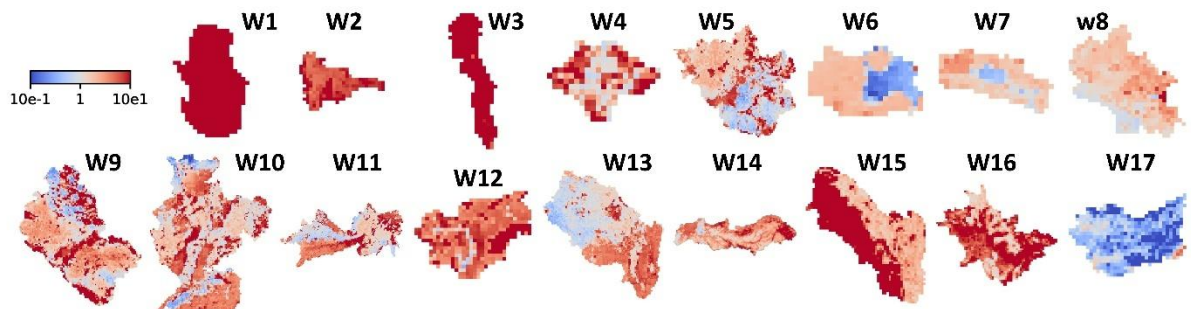
(a) Nitrogen inputs [kg/ha yr]



(b) Soil denitrification [kg/ha yr]



(c) Damköhler number [-]



829

830 Figure 10. The simulated long-term average (1982-2024) of nitrogen inputs, soil denitrification, and
831 Damköhler number.

832

833

834 **Tables**

835 Table 1. Characteristics of the selected catchments. **Lat** depicts the latitude of upper left corner of the
 836 catchment. **DEM** and **Area** are the mean elevation in m.a.s.l. and catchment size in km². **Precip**, **Temp**,
 837 and **PET** are the annual averages of precipitation, air temperature, and potential evapotranspiration
 838 in mm/yr. f_{crop} , f_{forest} , and f_{urban} are the fractions of cropland, forest, and urbanized areas in 2019
 839 in %. Null means no name is assigned for the catchment in the Catchment Characterisation and
 840 Modelling (CCM) database.

<u>ID</u>	<u>Name</u>	<u>Lat</u>	<u>Area</u>	<u>DEM</u>	<u>Precip</u>	<u>Temp</u>	<u>PET</u>	<u>f_{crop}</u>	<u>f_{forest}</u>	<u>f_{urban}</u>
<u>1</u>	<u>Null</u>	<u>70.0</u>	<u>8725</u>	<u>468.5</u>	<u>448.5</u>	<u>-1.8</u>	<u>442.8</u>	<u><1</u>	<u>1.9</u>	<u><1</u>
<u>2</u>	<u>Vefsna</u>	<u>65.9</u>	<u>5475</u>	<u>636.5</u>	<u>1260.8</u>	<u>0.7</u>	<u>433.6</u>	<u><1</u>	<u>24.6</u>	<u><1</u>
<u>3</u>	<u>Null</u>	<u>59.8</u>	<u>5225</u>	<u>742.3</u>	<u>1400.9</u>	<u>3.0</u>	<u>545.7</u>	<u><1</u>	<u>39.8</u>	<u><1</u>
<u>4</u>	<u>Null</u>	<u>58.3</u>	<u>4350</u>	<u>67.4</u>	<u>654.5</u>	<u>6.4</u>	<u>667.9</u>	<u>17.4</u>	<u>60.5</u>	<u>1.4</u>
<u>5</u>	<u>Nemunas</u>	<u>56.6</u>	<u>97550</u>	<u>147.9</u>	<u>599.3</u>	<u>7.1</u>	<u>730.6</u>	<u>33.0</u>	<u>39.1</u>	<u>4.5</u>
<u>6</u>	<u>Tweed</u>	<u>55.9</u>	<u>6250</u>	<u>264.3</u>	<u>1023.4</u>	<u>7.9</u>	<u>600.9</u>	<u>21.8</u>	<u>18.9</u>	<u>1.4</u>
<u>7</u>	<u>Null</u>	<u>52.3</u>	<u>4300</u>	<u>175.4</u>	<u>1218.1</u>	<u>10.1</u>	<u>645.2</u>	<u>12.1</u>	<u>17.4</u>	<u>1.9</u>
<u>8</u>	<u>Thames</u>	<u>52.2</u>	<u>11900</u>	<u>112.0</u>	<u>700.7</u>	<u>10.4</u>	<u>782.9</u>	<u>44.9</u>	<u>14.1</u>	<u>22.0</u>
<u>9</u>	<u>Elbe</u>	<u>53.5</u>	<u>130225</u>	<u>318.3</u>	<u>626.9</u>	<u>8.8</u>	<u>836.3</u>	<u>41.2</u>	<u>34.6</u>	<u>10.8</u>
<u>10</u>	<u>Rhine</u>	<u>52.0</u>	<u>170175</u>	<u>508.3</u>	<u>943.3</u>	<u>8.9</u>	<u>821.0</u>	<u>21.5</u>	<u>41.2</u>	<u>17.1</u>
<u>11</u>	<u>Danube(a)</u>	<u>50.5</u>	<u>197600</u>	<u>618.0</u>	<u>843.6</u>	<u>8.3</u>	<u>857.4</u>	<u>28.5</u>	<u>37.1</u>	<u>11.5</u>
<u>12</u>	<u>Adige</u>	<u>47.2</u>	<u>11600</u>	<u>1771.9</u>	<u>1002.3</u>	<u>4.5</u>	<u>809.7</u>	<u><1</u>	<u>48.8</u>	<u>3.2</u>
<u>13</u>	<u>Loire</u>	<u>48.7</u>	<u>122125</u>	<u>298.9</u>	<u>778.7</u>	<u>11.0</u>	<u>887.4</u>	<u>37.6</u>	<u>25.7</u>	<u>6.5</u>
<u>14</u>	<u>Tajo</u>	<u>40.4</u>	<u>75575</u>	<u>686.2</u>	<u>549.5</u>	<u>14.3</u>	<u>1359.6</u>	<u>26.7</u>	<u>34.5</u>	<u>3.3</u>
<u>15</u>	<u>Danube(b)</u>	<u>48.4</u>	<u>37975</u>	<u>533.3</u>	<u>534.7</u>	<u>8.1</u>	<u>869.5</u>	<u>32.0</u>	<u>41.3</u>	<u>6.4</u>
<u>16</u>	<u>Danube(c)</u>	<u>44.8</u>	<u>37725</u>	<u>653.3</u>	<u>684.7</u>	<u>9.7</u>	<u>994.2</u>	<u>12.8</u>	<u>44.3</u>	<u>5.8</u>
<u>17</u>	<u>Null</u>	<u>37.6</u>	<u>12650</u>	<u>1384.5</u>	<u>454.1</u>	<u>12.2</u>	<u>1256.9</u>	<u>5.9</u>	<u>4.3</u>	<u><1</u>

841

842

843 Table 2. The calibration performance of discharge (Q), in-stream isotopes (¹⁸O, Iso), and nitrate (NO³-
 844 N). Evaluation metrics include Kling-Gupta efficiency (KGE, -), Root Mean Square Error (RMSE; m3/s, ‰,
 845 and mg/L for discharge, isotopes, and nitrate, respectively), Pearson Correlation Coefficient
 846 (Coefficient; -), and Percent bias (Pbias; %).

Metric	Min	Max	Mean	Median
<u>KGE (Q)</u>	<u>0.14</u>	<u>0.89</u>	<u>0.65</u>	<u>0.69</u>
<u>KGE (Iso)</u>	<u>-0.03</u>	<u>0.86</u>	<u>0.45</u>	<u>0.48</u>
<u>KGE (NO³-N)</u>	<u>-0.36</u>	<u>0.72</u>	<u>0.42</u>	<u>0.44</u>
<u>Correlation (Q)</u>	<u>0.49</u>	<u>0.92</u>	<u>0.79</u>	<u>0.81</u>
<u>Correlation (Iso)</u>	<u>0.14</u>	<u>0.87</u>	<u>0.51</u>	<u>0.54</u>
<u>Correlation (NO³-N)</u>	<u>-0.26</u>	<u>0.86</u>	<u>0.55</u>	<u>0.6</u>
<u>RMSE (Q)</u>	<u>3.99</u>	<u>677.08</u>	<u>123.02</u>	<u>68.51</u>
<u>RMSE (Iso)</u>	<u>0.31</u>	<u>1.51</u>	<u>0.72</u>	<u>0.73</u>
<u>RMSE (NO³-N)</u>	<u>0.02</u>	<u>2.82</u>	<u>0.83</u>	<u>0.57</u>
<u>Pbias (Q)</u>	<u>0.52</u>	<u>79.88</u>	<u>17.44</u>	<u>9.53</u>
<u>Pbias (Iso)</u>	<u>-11.28</u>	<u>-0.07</u>	<u>-4.3</u>	<u>-4.42</u>
<u>Pbias (NO³-N)</u>	<u>0.18</u>	<u>49.25</u>	<u>15.52</u>	<u>10.89</u>

847

848

849 **Reference**

- 850 Akbarzadeh, Z., Maavara, T., Slowinski, S., & Van Cappellen, P. (2019). Effects of Damming on River
851 Nitrogen Fluxes: A Global Analysis. *Global Biogeochemical Cycles*, 33.
852 <https://doi.org/10.1029/2019GB006222>
- 853 Ala-aho, P., Tetzlaff, D., Mcnamara, J., Laudon, H., & Kormos, P. (2017). Modeling the isotopic
854 evolution of snowpack and snowmelt: Testing a spatially distributed parsimonious approach.
855 *Water Resources Research*, 53. <https://doi.org/10.1002/2017WR020650>
- 856 Amato, M. T., & Giménez, D. (2024). Predicting monthly near-surface soil temperature from air
857 temperature and the leaf area index. *Agricultural and Forest Meteorology*, 345, 109838.
858 <https://doi.org/10.1016/j.agrformet.2023.109838>
- 859 Arnold, J., Moriasi, D., Gassman, P., Abbaspour, K., White, M., Srinivasan, R., et al. (2012). SWAT:
860 Model use, calibration, and validation. *Transactions of the ASABE (American Society of*
861 *Agricultural and Biological Engineers)*, 55. <https://doi.org/10.13031/2013.42256>
- 862 Bajracharya, A., Moghairib, M., Stadyk, T., & Asadzadeh, M. (2023). Process based calibration of a
863 continental-scale hydrological model using soil moisture and streamflow data. *Journal of*
864 *Hydrology: Regional Studies*, 47, 101391. <https://doi.org/10.1016/j.ejrh.2023.101391>
- 865 Benettin, P., Bailey, S., Campbell, J., Green, M., Rinaldo, A., Likens, G., et al. (2015). Linking water age
866 and solute dynamics in streamflow at the Hubbard Brook Experimental Forest, NH, USA.
867 *Water Resources Research*, 51, [n/a-n/a9256–9272](https://doi.org/10.1002/2015WR017552). <https://doi.org/10.1002/2015WR017552>
- 868 Beven, K. (2006). A manifesto for the equifinality thesis. *Journal of Hydrology*, 320(1–2), 18–36.
869 <https://doi.org/10.1016/J.JHYDROL.2005.07.007>
- 870 Beven, K. (2015). Facets of uncertainty: Epistemic uncertainty, non-stationarity, likelihood, hypothesis
871 testing, and communication. *Hydrological Sciences Journal*, 61, 150407155940006.
872 <https://doi.org/10.1080/02626667.2015.1031761>
- 873 Birkel, C., & Soulsby, C. (2015). Advancing tracer-aided rainfall-runoff modelling: A review of progress,
874 problems and unrealised potential. *Hydrological Processes*, 29(25), 5227–5240.
875 <https://doi.org/10.1002/HYP.10594>
- 876 Birkel, C., Tetzlaff, D., & Dunn, S. (2011). Using time domain and geographic source tracers to
877 conceptualize streamflow generation processes in lumped rainfall-runoff models. *Water*
878 *Resources Research - WATER RESOUR RES*, 47. <https://doi.org/10.1029/2010WR009547>
- 879 Bonchkovskiy, A., & Osadcha, N. (2024). Modelling of the nutrient load in the Sula River basin using
880 the MONERIS. *Physical Geography and Geomorphology*, 47, 7–20.
881 <https://doi.org/10.17721/phgg.2024.3-4.01>
- 882 Condon, L., Kollet, S., Bierkens, M., Maxwell, R., Hill, M., Franssen, H.-J., et al. (2021). Global
883 Groundwater Modeling and Monitoring: Opportunities and Challenges. *Water Resources*
884 *Research*, 57. <https://doi.org/10.1029/2020WR029500>
- 885 Craig, H., Gordon, L. I., & Horibe, Y. (1964). Isotopic exchange effects in the evaporation of water: 1.
886 Low-temperature experimental results. *Journal of Geophysical Research*, 68(17), 5079–5087.
887 <https://doi.org/10.1029/JZ068I017P05079>
- 888 Dawson, T., & Ehleringer, J. (1991). Streamside trees that do not use stream water. *Nature*, 350, 335–
889 337. <https://doi.org/10.1038/350335a0>
- 890 Dick, J. J., Tetzlaff, D., Birkel, C., & Soulsby, C. (2015). Modelling landscape controls on dissolved
891 organic carbon sources and fluxes to streams. *Biogeochemistry*, 122(2–3), 361–374.
892 <https://doi.org/10.1007/S10533-014-0046-3>
- 893 [Donnelly, C., Andersson, J.M., & Arheimer, B. \(2016\). Using flow signatures and catchment similarities](https://doi.org/10.1080/02626667.2015.1027710)
894 [to evaluate the E-HYPE multi-basin model across Europe. *Hydrological Sciences Journal*, 61\(2\),](https://doi.org/10.1080/02626667.2015.1027710)
895 [255–273. https://doi.org/10.1080/02626667.2015.1027710](https://doi.org/10.1080/02626667.2015.1027710)

896 Eckersten, H., Jansson, P. E., & Johnsson, H. (1994). SOILN model – user’s manual 2nd edition, Division
897 of Agricultural Hydrotechnics Communications, 94:4. Department of Soil Sciences, Swedish
898 University of Agricultural Sciences, 58pp, Uppsala.

899 Efstratiadis, A., & Koutsoyiannis, D. (2010). One decade of multi-objective calibration approaches in
900 hydrological modelling: A review. *Hydrological Sciences Journal*, 55(1), 58–78.
901 <https://doi.org/10.1080/02626660903526292>

902 Godsey, S. E., Aas, W., Clair, T. A., de Wit, H. A., Fernandez, I. J., Kahl, J. S., et al. (2010). Generality of
903 fractal 1/f scaling in catchment tracer time series, and its implications for catchment travel
904 time distributions. *Hydrological Processes*, 24(12), 1660–1671.
905 <https://doi.org/10.1002/hyp.7677>

906 Good, S. P., Soderberg, K., Guan, K., King, E. G., Scanlon, T. M., & Caylor, K. K. (2014). $\delta^2\text{H}$ isotopic flux
907 partitioning of evapotranspiration over a grass field following a water pulse and subsequent
908 dry down. *Water Resources Research*, 50(2), 1410–1432.
909 <https://doi.org/10.1002/2013WR014333>

910 Grizzetti, B., Vigiak, O., Udias, A., Aloe, A., Zanni, M., Bouraoui, F., et al. (2021). How EU policies could
911 reduce nutrient pollution in European inland and coastal waters. *Global Environmental*
912 *Change*, 69, 102281. <https://doi.org/10.1016/j.gloenvcha.2021.102281>

913 Hooper, R., Stone, A., Christophersen, N., de Melo, E., & Seip, H. (1988). Assessing the Birkenes Model
914 of Stream Acidification using a multi-signal calibration methodology. *Water Resources*
915 *Research - WATER RESOUR RES*, 24, 1308–1316. <https://doi.org/10.1029/WR024i008p01308>

916 Horita, J., Rozanski, K., & Cohen, S. (2008). Isotope effects in the evaporation of water: A status report
917 of the Craig-Gordon model. *Isotopes in Environmental and Health Studies*, 44, 23–49.
918 <https://doi.org/10.1080/10256010801887174>

919 Hrachowitz, M., Savenije, H., Bogaard, T. A., Tetzlaff, D., & Soulsby, C. (2013). What can flux tracking
920 teach us about water age distribution patterns and their temporal dynamics? *Hydrology and*
921 *Earth System Sciences*, 17(2), 533–564. <https://doi.org/10.5194/HESS-17-533-2013>

922 Huijgevoort, M., Tetzlaff, D., & Sutanudjaja, E. (2016). Using high resolution tracer data to constrain
923 water storage, flux and age estimates in a spatially distributed rainfall-runoff model.
924 *Hydrological Processes*, 30. <https://doi.org/10.1002/hyp.10902>

925 Jasechko, S., Kirchner, J., Welker, J., & McDonnell, J. (2016). Substantial proportion of global
926 streamflow less than three months old. *Nature Geoscience*, 9.
927 <https://doi.org/10.1038/NGEO2636>

928 [Jones, E. R., Bierkens, M. F. P., Wanders, N., Sutanudjaja, E. H., van Beek, L. P. H., & van Vliet, M. T. H.](https://doi.org/10.5194/gmd-16-4481-2023)
929 [\(2023\). DynQual v1.0: a high-resolution global surface water quality model. *Geoscientific*](https://doi.org/10.5194/gmd-16-4481-2023)
930 [*Model Development*, 16\(15\), 4481–4500. https://doi.org/10.5194/gmd-16-4481-2023](https://doi.org/10.5194/gmd-16-4481-2023)

931 Jung, H., Tetzlaff, D., Birkel, C., & Soulsby, C. (2025). Recent Developments and Emerging Challenges
932 in Tracer-Aided Modeling. *Wiley Interdisciplinary Reviews Water*, 12.
933 <https://doi.org/10.1002/wat2.70015>

934 Kale, R., & Sahoo, B. (2011). Green-Ampt Infiltration Models for Varied Field Conditions: A Revisit.
935 *Water Resources Management*, 25, 3505–3536. <https://doi.org/10.1007/s11269-011-9868-0>

936 Kumar, R., Samaniego, L., & Attinger, S. (2013). Implications of distributed hydrologic model
937 parameterization on water fluxes at multiple scales and locations. *Water Resources Research*,
938 49(1), 360–379. <https://doi.org/10.1029/2012WR012195>

939 Kuppel, S., Tetzlaff, D., Maneta, M., & Soulsby, C. (2018). ECH2O-iso 1.0: Water isotopes and age
940 tracking in a process-based, distributed ecohydrological model. *Geoscientific Model*
941 *Development*, 11, 3045–3069. <https://doi.org/10.5194/gmd-11-3045-2018>

- 942 Landgraf, J., Tetzlaff, D., Birkel, C., Stevenson, J., & Soulsby, C. (2023). Assessing land use effects on
 943 ecohydrological partitioning in the critical zone through isotope-aided modelling. *Earth*
 944 *Surface Processes and Landforms*, 48. <https://doi.org/10.1002/esp.5691>
- 945 Lindström, G., Pers, C., Rosberg, J., Strömqvist, J., & Arheimer, B. (2010). Development and test of the
 946 HYPE (Hydrological Predictions for the Environment) model – A water quality model for
 947 different spatial scales. *Hydrology Research*, 41. <https://doi.org/10.2166/nh.2010.007>
- 948 Maneta, M. P., & Silverman, N. L. (2013). A spatially distributed model to simulate water, energy, and
 949 vegetation dynamics using information from regional climate models. *Earth Interactions*,
 950 17(11), 1–44. <https://doi.org/10.1175/2012Ei000472.1>
- 951 McDonnell, J. (2014). The two water worlds hypothesis: Ecohydrological separation of water between
 952 streams and trees? *Wiley Interdisciplinary Reviews: Water*, 1.
 953 <https://doi.org/10.1002/wat2.1027>
- 954 McDonnell, J., & Beven, K. (2014). Debates on Water Resources: The future of hydrological sciences:
 955 A (common) path forward? A call to action aimed at understanding velocities, celerities and
 956 residence time distributions of the headwater hydrograph. *Water Resources Research*, 50.
 957 <https://doi.org/10.1002/2013WR015141>
- 958 Mcmillan, H., Araki, R., Bolotin, L., Kim, D.-H., Coxon, G., Clark, M., & Seibert, J. (2025). Global patterns
 959 in observed hydrologic processes. *Nature Water*, 3. [https://doi.org/10.1038/s44221-025-](https://doi.org/10.1038/s44221-025-00407-w)
 960 [00407-w](https://doi.org/10.1038/s44221-025-00407-w)
- 961 Mikayilov, F., Rouholahnejad Freund, E., Ashraf Vaghefi, S., Srinivasan, R., Yang, H., & Klöve, B. (2015).
 962 A continental-scale hydrology and water quality model for Europe: Calibration and uncertainty
 963 of a high-resolution large-scale SWAT model. *Journal of Hydrology*, 524.
 964 <https://doi.org/10.1016/j.jhydrol.2015.03.027>
- 965 Nan, Y., He, Z., Tian, F., Wei, Z., & Tian, L. (2021). Can we use precipitation isotope outputs of isotopic
 966 general circulation models to improve hydrological modeling in large mountainous
 967 catchments on the Tibetan Plateau? *Hydrology and Earth System Sciences*, 25(12), 6151–6172.
 968 <https://doi.org/10.5194/hess-25-6151-2021>
- 969 [Naz, B. Sharples, W., Ma, Y., Goergen, K., & Kollet, S. \(2023\). Continental-scale evaluation of a fully](https://doi.org/10.5194/gmd-16-1617-2023)
 970 [distributed coupled land surface and groundwater model, ParFlow-CLM \(v3.6.0\), over Europe.](https://doi.org/10.5194/gmd-16-1617-2023)
 971 [Geoscientific Model Development, 16\(6\), 1617–1639. https://doi.org/10.5194/gmd-16-1617-](https://doi.org/10.5194/gmd-16-1617-2023)
 972 [2023](https://doi.org/10.5194/gmd-16-1617-2023)
- 973 Neal, C., Christophersen, N., Neale, R., Smith, C., & Reynolds, B. (1988). Chloride in precipitation and
 974 streamwater for the upland catchment of River Severn, mid- Wales; some consequences for
 975 hydrochemical models. *Hydrological Processes*, 2, 155–165.
 976 <https://doi.org/10.1002/hyp.3360020206>
- 977 Nearing, G., Ruddell, B., Bennett, A., Prieto, C., & Gupta, H. (2020). Does Information Theory Provide
 978 a New Paradigm for Earth Science? Hypothesis Testing. *Water Resources Research*, 56.
 979 <https://doi.org/10.1029/2019WR024918>
- 980 Ocampo, C., Sivapalan, M., & Oldham, C. (2006). Hydrological connectivity of upland-riparian zones in
 981 agricultural catchments: Implications for runoff generation and nitrate transport. *Journal of*
 982 *Hydrology*, 331, 643–658. <https://doi.org/10.1016/j.jhydrol.2006.06.010>
- 983 Pechlivanidis, I., Jackson, B., Mcintyre, N., & Wheeler, H. (2011). Catchment scale hydrological
 984 modelling: A review of model types, calibration approaches and uncertainty analysis methods
 985 in the context of recent developments in technology and applications. *GlobalNEST*
 986 *International Journal*, 13, 193–214.
- 987 Pesántez, J., Birkel, C., Gaona, G., Arciniega-Esparza, S., Murray, D., Mosquera, G., et al. (2023).
 988 Spatially distributed tracer-aided modelling to explore DOC dynamics, hot spots and hot
 989 moments in a tropical mountain catchment. *Hydrological Processes*, 37, 1–15.
 990 <https://doi.org/10.1002/hyp.15020>

991 Rakovec, O., Kumar, R., Mai, J., Cuntz, M., Thober, S., Zink, M., et al. (2016). Multiscale and Multivariate
992 Evaluation of Water Fluxes and States over European River Basins. *Journal of*
993 *Hydrometeorology*, 17, 287–307. <https://doi.org/10.1175/JHM-D-15-0054.1>

994 Rakovec, O., Mizukami, N., Kumar, R., Newman, A., Thober, S., Wood, A., et al. (2019). Diagnostic
995 Evaluation of Large-Domain Hydrologic Models Calibrated Across the Contiguous United
996 States. *Journal of Geophysical Research: Atmospheres*, 124.
997 <https://doi.org/10.1029/2019JD030767>

998 Remondi, F., Kirchner, J., Burlando, P., & Fatichi, S. (2018). Water Flux Tracking with A Distributed
999 Hydrological Model to Quantify Controls on the Spatio-Temporal Variability of Transit Time
1000 Distributions. *Water Resources Research*, 54. <https://doi.org/10.1002/2017WR021689>

1001 Samaniego, L., Kumar, R., & Attinger, S. (2010). Multiscale parameter regionalization of a grid-based
1002 hydrologic model at the mesoscale. *Water Resour. Res.*, 46.
1003 <https://doi.org/10.1029/2008WR007327>

1004 Seybold, E., Dwivedi, R., Musselman, K., Kincaid, D., Schroth, A., Classen, A., et al. (2022). Winter runoff
1005 events pose an unquantified continental-scale risk of high wintertime nutrient export.
1006 *Environmental Research Letters*, 17, 104044. <https://doi.org/10.1088/1748-9326/ac8be5>

1007 Šimůnek, J., Šejna, M., Saito, H., & Van Genuchten, M. T. (2013). *The HYDRUS-1D software package*
1008 *for simulating the one-dimensional movement of water, heat, and multiple solutes in variably-*
1009 *saturated media (Version 4.17)*. Department of Environmental Sciences University of Riverside
1010 California, California.

1011 Skrzypek, G., Mydłowski, A., Dogramaci, S., Hedley, P., Gibson, J. J., & Grierson, P. F. (2015). Estimation
1012 of evaporative loss based on the stable isotope composition of water using Hydrocalculator.
1013 *Journal of Hydrology*, 523, 781–789. <https://doi.org/10.1016/j.jhydrol.2015.02.010>

1014 Smith, A., Tetzlaff, D., Kleine, L., Maneta, M., & Soulsby, C. (2021). Quantifying the effects of land use
1015 and model scale on water partitioning and water ages using tracer-aided ecohydrological
1016 models. *Hydrology and Earth System Sciences*, 25, 2239–2259. [https://doi.org/10.5194/hess-](https://doi.org/10.5194/hess-25-2239-2021)
1017 [25-2239-2021](https://doi.org/10.5194/hess-25-2239-2021)

1018 Soulsby, C., Birkel, C., Geris, J., Dick, J., Tunaley, C., & Tetzlaff, D. (2015). Stream water age distributions
1019 controlled by storage dynamics and nonlinear hydrologic connectivity: Modeling with high-
1020 resolution isotope data. *Water Resources Research*, 51(9), 7759–7776.
1021 <https://doi.org/10.1002/2015WR017888>

1022 Sprenger, M., Stumpp, C., Weiler, M., Aeschbach, W., Allen, S., Benettin, P., et al. (2019). The
1023 Demographics of Water: A Review of Water Ages in the Critical Zone. *Reviews of Geophysics*,
1024 57. <https://doi.org/10.1029/2018RG000633>

1025 Tetzlaff, D., Buttle, J., Carey, S. K., Mcguire, K., Laudon, H., & Soulsby, C. (2015). Tracer-based
1026 assessment of flow paths, storage and runoff generation in northern catchments: A review.
1027 *Hydrological Processes*, 29(16), 3475–3490. <https://doi.org/10.1002/HYP.10412>

1028 Wang, J., Bouwman, A., Vilmin, L., Beusen, A., Hoek, W., Liu, X., & Middelburg, J. (2024). Global inland-
1029 water nitrogen cycling has accelerated in the Anthropocene. *Nature Water*, 2.
1030 <https://doi.org/10.1038/s44221-024-00282-x>

1031 Wellen, C., Kamran-Disfani, A.-R., & Arhonditsis, G. (2015). Evaluation of the Current State of
1032 Distributed Watershed Nutrient Water Quality Modeling. *Environmental Science &*
1033 *Technology*, 49. <https://doi.org/10.1021/es5049557>

1034 Wen, Y., Lin, J.-S., Plaza, F., & Liang, X. (2024). Roles of Hydrology and Transport Processes in
1035 Denitrification at Watershed Scale. *Water Resources Research*, 60, 1–24.
1036 <https://doi.org/10.1029/2023WR034971>

1037 Winkler, K., Fuchs, R., Rounsevell, M., & Herold, M. (2021). Global land use changes are four times
1038 greater than previously estimated. *Nature Communications*, 12(1), 2501.
1039 <https://doi.org/10.1038/s41467-021-22702-2>

1040 Wu, S., Tetzlaff, D., Yang, X., & Soulsby, C. (2022). Disentangling the influence of landscape
1041 characteristics, hydroclimatic variability and land management on surface water NO₃-N
1042 dynamics: spatially distributed modelling over 30 years in a lowland mixed land use catchment.
1043 *Water Resources Research*, e2021WR030566. <https://doi.org/10.1029/2021WR030566>

1044 Wu, S., Tetzlaff, D., Beven, K., & Soulsby, C. (2025a). DREAM(LoAX): Simultaneous Calibration and
1045 Diagnosis for Tracer-Aided Ecohydrological Models Under the Equifinality Thesis. *Water*
1046 *Resources Research*, 61, e2024WR038779. <https://doi.org/10.1029/2024WR038779>

1047 Wu, S., Tetzlaff, D., Yang, X., Sauter, T., & Soulsby, C. (2025b). Hydrological Connectivity Dominates
1048 NO₃-N Cycling in Complex Landscapes – Insights From Integration of Isotopes and Water
1049 Quality Modeling. *Water Resources Research*, 61, [e2025WR040525](https://doi.org/10.1029/2025WR040525).
1050 <https://doi.org/10.1029/2025WR040525>

1051 Wu, S., Tetzlaff, D., & Soulsby, C. (2025c). Revising Common Approaches for Calibration: Insights From
1052 a 1-D Tracer-Aided Hydrological Model With High-Dimensional Parameters and Objectives.
1053 *Water Resources Research*, 61, e2024WR037656. <https://doi.org/10.1029/2024WR037656>

1054 Wu, S., Tetzlaff, D., Zheng, Y., & Soulsby, C. (2025d). EcoTWIN v1.0 release.
1055 <https://doi.org/10.5281/zenodo.16747633>

1056 Yang, C., Condon, L., & Maxwell, R. (2025). Unravelling groundwater–stream connections over the
1057 continental United States. *Nature Water*, 3. <https://doi.org/10.1038/s44221-024-00366-8>

1058 Yang, X., Jomaa, S., Zink, M., Fleckenstein, J., Borchardt, D., & Rode, M. (2018). A New Fully Distributed
1059 Model of Nitrate Transport and Removal at Catchment Scale. *Water Resources Research*, 54.
1060 <https://doi.org/10.1029/2017WR022380>

1061 Yang, X., Zhang, X., Graeber, D., Hensley, R., Jarvie, H., Lorke, A., et al. (2023a). Large-stream nitrate
1062 retention patterns shift during droughts: Seasonal to sub-daily insights from high-frequency
1063 data-model fusion. *Water Research*, 243, 120347.
1064 <https://doi.org/10.1016/j.watres.2023.120347>

1065 Yang, X., Tetzlaff, D., Müller, C., Knöller, K., Borchardt, D., & Soulsby, C. (2023b). Upscaling Tracer-
1066 Aided Ecohydrological Modeling to Larger Catchments: Implications for Process
1067 Representation and Heterogeneity in Landscape Organization. *Water Resources Research*, 59,
1068 e2022WR033033. <https://doi.org/10.1029/2022WR033033>

1069 Yang, X., Tetzlaff, D., Jin, J., Li, Q., Borchardt, D., & Soulsby, C. (2024). Linking terrestrial biogeochemical
1070 processes and water ages to catchment water quality: A new Damköhler analysis based on
1071 coupled modeling of isotope tracers and nitrate dynamics. *Water Research*, 262, 122118.
1072 <https://doi.org/10.1016/j.watres.2024.122118>

1073 Zhang, Z., Chen, X., Cheng, Q.-B., Li, S.-L., Yue, F.-J., Peng, T., et al. (2020). Coupled hydrological and
1074 biogeochemical modelling of nitrogen transport in the karst critical zone. *Science of The Total*
1075 *Environment*, 732, 138902. <https://doi.org/10.1016/j.scitotenv.2020.138902>

1076 Zhu, J., Jia, Y., Yu, G., Wang, Q., He, N., Chen, Z., et al. (2025). Changing patterns of global nitrogen
1077 deposition driven by socio-economic development. *Nature Communications*, 16(1), 46.
1078 <https://doi.org/10.1038/s41467-024-55606-y>

1079